

INVITED CENTENNIAL ARTICLE

Metamorphic chronology—a tool for all ages: Past achievements and future prospects

MATTHEW J. KOHN^{1,*}

¹Department of Geosciences, Boise State University, Boise, Idaho 83725, U.S.A.

ABSTRACT



Metamorphic chronology or petrochronology has steadily evolved over several decades through ever improving analytical techniques and more complete understanding of the geochemical and petrologic evolution of metamorphosing rocks. Here, the principal methods by which we link metamorphic temperatures (T) and ages (t) are reviewed, focusing primarily on accessory minerals. Methods discussed include textural correlation, inversion of diffusion profiles, chemical correlation, and combined chronologic and thermometric microanalysis. Each method demonstrates remarkable

power in elucidating petrologic and tectonic processes, as examples from several orogens illustrate, but limitations must also be acknowledged and help define future research directions. Correlation methods are conceptually simple, but can be relatively non-specific regarding pressure-temperature conditions of formation. A new consideration of errors indicates that modeling of chronologic diffusion gradients provides relatively precise constraints on cooling rates, whereas models of chemical diffusion gradients can lead to large (factor of 2 or more) cooling rate uncertainties. Although arguably the best method currently in use, simultaneous T - t measurements are currently limited to zircon, titanite, and rutile. Directions for future improvement include investigation of diffusion profiles for numerous trace element-mineral systems using now-routine depth profiling. New trace element models will help improve chemical correlation methods. The determination of inclusion entrapment P - T conditions based on Raman spectroscopic measurement of inclusion pressures (“thermoba-Raman-try”) may well revolutionize textural correlation methods.

Keywords: Geochronology, monazite, titanite, zircon, trace elements and REE, Zr, zircon, titanite, rutile, metamorphic petrology, UHP, Invited Centennial article

INTRODUCTION

Understanding Earth processes commonly depends on constraining rates. Although the aphorism “*No dates, no rates*” is disproved by modeling chemical diffusion profiles (see below), improvements in how we date minerals have indeed led to many major advances in petrogenesis and tectonics. In the last couple decades, metamorphic geochronologists have increasingly sought to develop new analytical and theoretical techniques to link ages with temperature and/or mineral reactions and petrologic evolution. Referred to as “petrochronology”¹ in some quarters, this integrative approach culminates a large body of research in metamorphic geochronology, mineral chemistry, and petrogenesis. This review considers four different ways in which we link metamorphic ages (“ t ”) with temperature (“ T ”), mainly in the context of accessory minerals: (1) textural correlation between

key minerals and ages; (2) inversion of diffusional zoning, both chemical zoning and chronologic zoning; (3) chemical correlation of ages to mineral growth events; and (4) simultaneous microanalysis of ages and trace-element temperatures in mineral domains. Examples, limitations, and advantages are discussed. Last, some views are presented on research directions with good future potential, including further development of geochemical tracers, new trace element models, and the use of Raman spectroscopy for determining inclusion pressures and temperatures (“thermoba-Raman-try”).

TEXTURAL CORRELATION

Datable inclusions in a petrogenetically diagnostic host

Many textural correlations rely on dating mineral inclusions inside a host mineral whose chemistry or growth is somehow linked to P - T evolution. The most common host mineral is garnet, both because it commonly grows with increasing P or T so its rim may represent the peak of metamorphism, and because its chemistry can be inverted to constrain a P - T path. Thus, the age for a garnet core vs. rim can inform rates of heating or loading, which can be useful for tectonic interpretations and models of mineral growth kinetics. Conceptually, if an accessory mineral continually reequilibrates during metamorphism,

* E-mail: mattkohn@boisestate.edu

¹ Engi (2009), but see also Fraser et al. (1997) for the first use in the geosciences literature. Originally (Thompson 1969), petrochronology was defined in reference to a Yoruba (west African) cult of the river god Eyinle, in which the number of stones in a ceremonial earthenware pot was proposed as a possible measure of duration and intensity of devotion, i.e., a sort of “stone-chronometer.” As Thompson wrote (p. 141): “Future research will determine whether there is a mean correlation between years and stones. If there is, we have a [method] for the dating of the pots, a science that we take the liberty of designating in advance petrochronology.”

either via recrystallization or diffusion, the measured age of inclusions at any point in a garnet gives the time of that stage of growth. Alternatively, if accessory minerals do not completely reequilibrate (e.g., if they retain relict cores), the youngest age at a radial position might be viewed as the best estimate of the host phase age at that point. Both views assume that, once included, an accessory mineral is inert to further reequilibration, both because it is isolated from the matrix, and because diffusivities for many elements in garnet are slow. It is further assumed that some mechanism drives continuous accessory mineral growth or recrystallization, a view that is rarely supported theoretically.

Textural correlation is conceptually simple but results are not always easy to interpret. Consider two rocks collected from near the main central thrust (MCT) in the central Himalaya investigated by Catlos et al. (2001). They used an ion microprobe to collect in situ $^{232}\text{Th}/^{208}\text{Pb}$ ages in monazite grains from different textural settings. In one rock (Fig. 1a), monazite inclusions in the rim of a garnet and matrix monazite grains show remarkably good age correspondence: essentially all ages are between 6 and 7 Ma. These data were interpreted to imply that monazite either reequilibrated during prograde metamorphism or grew near the metamorphic peak, so the age of peak metamorphism, as reflected by final growth of the garnet and matrix monazite grains, occurred about 6–7 Ma. This interpretation makes sense in a regional context because monazite ages are systematically older in structurally higher rocks and systematically younger in structurally lower rocks. But without identifying a specific monazite-forming reaction from thermodynamic modeling (Spear and Pyle 2010; Spear 2010) or the temperature of monazite formation from trace element thermometry (Pyle et al. 2001), the likelihood that both garnet and monazite grew near the peak of metamorphism cannot be assessed, and in fact for many bulk-rock compositions monazite should dissolve as garnet grows (Spear and Pyle 2010). Thus, presuming the garnet rim grew near the peak of metamorphism, the monazite age provides a maximum rather

than direct constraint (i.e., peak metamorphism occurred $\leq 6\text{--}7$ Ma). A minimum constraint is derived from muscovite $^{40}\text{Ar}/^{39}\text{Ar}$ cooling ages of 4–5 Ma from the same structural level (Catlos et al. 2001). Overall, a relatively tight constraint on the peak of metamorphism is possible in this area (6 ± 1 Ma) through combined chronometers.

A second rock from the next higher thrust sheet illustrates greater age complexities and ambiguities using textural correlation alone. Matrix grain ages range from 11 to 29 Ma, and an inclusion near the rim of the garnet is ≥ 30 Ma. These data were interpreted to reflect early prograde metamorphism, with late-stage resetting leading to the 11 Ma age. At the time, the closure temperature of monazite to Pb loss was thought to be 600–650 °C (Smith and Giletti 1997), and the peak temperature of the rock was ca. 750 °C, so 11 Ma was thought to provide a minimum estimate of the age of peak metamorphism. Although Catlos et al.'s interpretation of these ages may be correct, the ages say little about the timing of peak metamorphism. Possibly it was ~ 11 Ma (the age of the youngest matrix monazite) or even younger, or perhaps as old as ~ 30 Ma (the age of the youngest inclusion in garnet). For an orogen whose lifetime spans < 60 Ma, a 20 Ma range in ages leads to considerable ambiguity in tectonic interpretations.

Would more data help? Hoisch et al. (2008) dated dozens of tiny monazite inclusions in several garnets from the Grouse Creek Range, Utah, to provide one of the most comprehensive data sets of spatially distributed ages (Fig. 2). Ages generally decrease toward garnet rims, but with greater scatter than expected from analytical error alone. Hoisch et al. (2008) interpreted the monazite ages as decreasing linearly with increasing volume of garnet (Fig. 2a), which implicitly requires that analytical errors are underestimated (by a factor of ~ 4). From a petrogenetic perspective, without any information about the monazite-forming reaction(s), inclusion ages provide maximum estimates of garnet growth ages, so do not directly constrain garnet growth

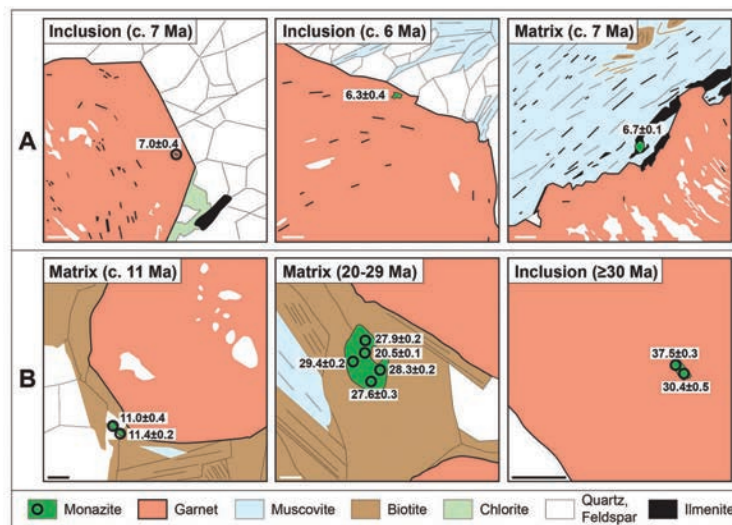


FIGURE 1. Textural correlation of monazite ages with metamorphic petrogenesis in Himalayan rocks, central Nepal (from Catlos et al. 2001). (a) Similar ages of monazite inclusions near garnet rim and matrix monazite are interpreted to represent the timing of the peak of metamorphism. (b) Disparate ages from inclusion and matrix grains are interpreted to represent early prograde metamorphism and late-stage recrystallization or resetting. Scale bars are all 100 μm . Black circles are analytical locations.

rates. Because garnet growth in many rocks is expected to drive monazite dissolution, not growth (Spear and Pyle 2010), the ages indicate that garnet growth occurred later than ~40 Ma and do not otherwise constrain the rate of garnet growth.

Even if one assumes that the youngest monazite age at any radial position does accurately date the age of garnet at that point, a wholly different interpretation of garnet growth rates is possible depending on how one views the data. Considering just one garnet (Fig. 2a), the youngest monazite inclusion ages might be interpreted as nearly constant near the core, gradually decreasing in the mid-region of the garnet, and nearly constant near the rim. This age distribution implies that garnet grew rapidly (core), then slowly (mid-region), then rapidly again (near-rim). In contrast, considering monazite inclusions from all garnets together (correlated through garnet major element chemistry), a different garnet growth pattern is derivable: slow-rapid-slow (Fig. 2b). These disparate views of garnet growth have little impact on tectonic models for the region, but span the range of perspectives on how minerals grow—either slowly and progressively (Hoisch et al. 2008) as temperature rises; or rapidly and abruptly (Fig. 2) as nucleation or growth kinetics are overstepped, or garnet-forming reactions are crossed (e.g., Walther and Wood 1984; Ague and Baxter 2007; see discussion of Pattison et al. 2011; Spear et al. 2014). As this example illustrates, inclusion ages can provide important tectonic constraints (peak metamorphism appears younger than 40 Ma), but resolving the dynamics of mineral growth requires more than just textural correlation.

Petrogenetically diagnostic inclusions in a datable host

A complementary approach to textural correlation relies on dating domains of a chronologically useful host mineral that contains inclusions of a petrogenetically useful mineral. Metamorphic zircons with diagnostic inclusions represent common targets for this type of analysis. Investigation of ultrahigh-pressure (UHP) rocks from the Kaghan region, Pakistan (Kaneko et al. 2003), exemplifies the power of this approach. Cathodoluminescence images of zircons show distinct domains, with an inner detrital or protolith core, a mantle that contains quartz inclusions, and a rim that contains coesite

inclusions (Fig. 3a). Ion microprobe analyses of zircon from the quartz-bearing domains average ~50 Ma, whereas analyses from the coesite-bearing domains average ~47 Ma (Fig. 3a). These ages are absolutely crucial to interpreting Himalayan tectonics because they unequivocally indicate subduction of the leading edge of the Indian plate to UHP conditions by 47 Ma. This age is quite close to the interred age of initiation of continent-continent collision (~55 Ma; e.g., Najman et al. 2010) and substantially predates peak metamorphism of the Himalayan metamorphic core (~20 Ma; e.g., see summary of Godin et al. 2006).

What more do these data say about crustal dynamics, e.g., heating and burial rates? Without any other information, zircon could have grown around quartz and coesite just as the rock crossed the quartz-coesite boundary, perhaps over a small temperature range of only 10 °C. If so, heating and loading rates were extremely slow: 10 °C/3 Ma ~3 °C/Ma (Fig. 3b). Alternatively, zircon could have grown around quartz at low-*T* and coesite at high-*T*, say 450 and 700 °C, respectively. If so, heating and loading rates were extremely fast: 150 °C/3 Ma = 50 °C/Ma (Fig. 3b). Although the importance of these ages on Himalayan tectonics is truly profound, elucidating finer details of petrogenesis and tectonics requires additional quantitative information on the *P-T* conditions of inclusion entrapment, either through identification of prograde zircon-forming reactions (although these are not predicted from mass balance; Kohn et al. 2015), or through independent thermobarometry such as Ti-in-zircon thermometry (Watson et al. 2006).

Inclusion reequilibration?

Not all inclusions or crystal interiors are inert to reequilibration. Dissolution-reprecipitation has been proposed to explain garnet textures and chemical zoning in garnet interiors in central Vermont (Hames and Menard 1993), Norway (Pollok et al. 2008), and Greece (Martin et al. 2011). Distinctive features include fluid inclusion clouds, chemically defined embayments of garnet cores, chemically and texturally isolated “islands” (relict cores), and cross-cutting chemical zones. Garnets from a rock in southern Chile show optical textures (Fig. 4a) and

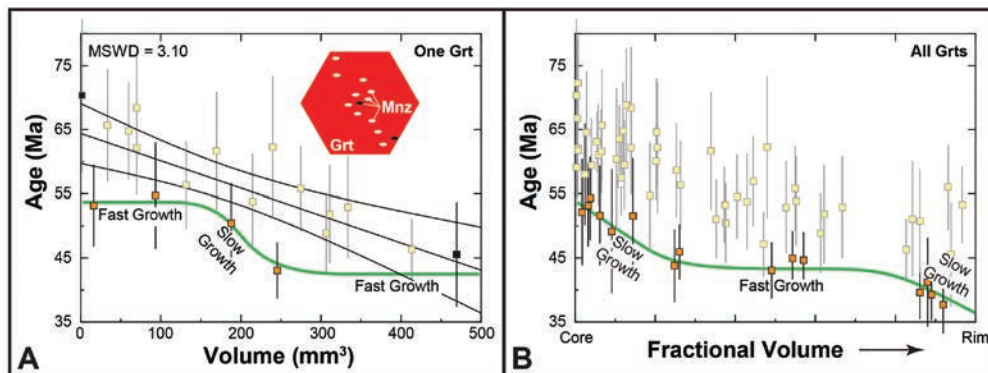


FIGURE 2. (a) Monazite inclusion chronology for single garnet from the Grouse Creek Mountains, NW Utah, showing a general decrease from core to rim (Hoisch et al. 2008). Inset shows schematically how monazites might be distributed through garnet; black monazite inclusions illustrate core vs. rim positions. Linear regression and 95% confidence limits (black lines) are for all data; green curve connecting young ages illustrates possible alternative growth history. Error bars are $\pm 2\sigma$. (b) All data from Hoisch et al. (2008) with possible alternative growth history connecting youngest inclusions.

chemical textures (Figs. 4b–4d) comparable to other studies, including fluid inclusion clouds, texturally and chemically isolated inclusions, and strong chemical zoning around inclusions (low Ca, high Mn) irrespective of radial position. Even if dissolution-precipitation is not the correct mechanism to explain these features, zoning in all major chemical components around inclusions demonstrates that the radial position is not a good indicator of relative timing—inclusions in the core and elsewhere are associated with garnet whose chemistry appears late. Of significance to this discussion, chemical and textural reequilibration is evident around seemingly isolated inclusions in the interior of the garnet. Sometimes healed fluid pathways connect inclusions with the matrix (Fig. 4a), but such textures are not always obvious (Fig. 4d). Other studies have argued for reequilibration of mineral inclusions, not just the host phase, e.g., formation of coesite inside zircon cores (Gebauer et al. 1997) and recrystallization of monazite inside garnets (Martin et al. 2007) but without obvious textural indicators like fluid inclusions. Thus, a mineral inclusion and its host may not always be isolated from later reequilibration, so textures alone do not always reliably link ages and petrogenesis.

Taken together, these studies caution that, although textural correlations can surely provide invaluable chronologic information, interpretations should be tempered with the realization that the ages provide limits only (not absolute P - T - t points), are not always very sensitive to P - T conditions, and may be affected by later processes. While it is always valuable to date mineral inclusions, or identify zones in datable minerals with distinct mineral inclusions, complementary supporting evidence for any interpretation should be marshaled.

DIFFUSION ZONING

Theory and errors

Diffusion zoning can be modeled to determine cooling rates in two different ways. Classically, chemical zoning is modeled in terms of diffusional exchange between a slow-diffusing host (usually garnet) and a fast-diffusing reservoir (usually biotite; Lasaga 1983). Taking garnet-biotite as an example, if Fe-Mg exchange is the sole reaction affecting compositions and volume diffusion within the garnet is the sole mechanism limiting that exchange, the compositions of garnet and matrix biotite can be inverted to obtain a closure temperature (T_c). The cooling rate (s , or “speed” of cooling) that is required to produce an observed T_c at a particular radial position is then calculated numerically (Fig. 5a). Faster cooling yields higher T_c values closer to the edge of the garnet, whereas slower cooling yields lower T_c values that penetrate farther into the garnet interior. Calculations are simplest if the mode of biotite is large, so it does not change composition, but other mode-dependent models are possible, albeit not considered here. An analogous example involving accessory minerals involves inversion of Zr zoning in rutile in the context of the Zr-in-rutile thermometer (Smye et al. 2014). Inversion of chemical diffusion profiles is wholly independent of chronologic measurements, i.e., rates can be determined independent of dates.

A complementary approach to the inversion of chemical zoning focuses on measuring chronologic zoning, typically with depth profiling. In this case, diffusion models infer T_c for each point, rather than s (Fig. 5b). Two different depths with different T_c values and ages provide an estimate of s , derived by dividing the difference in calculated T_c values by their difference in age

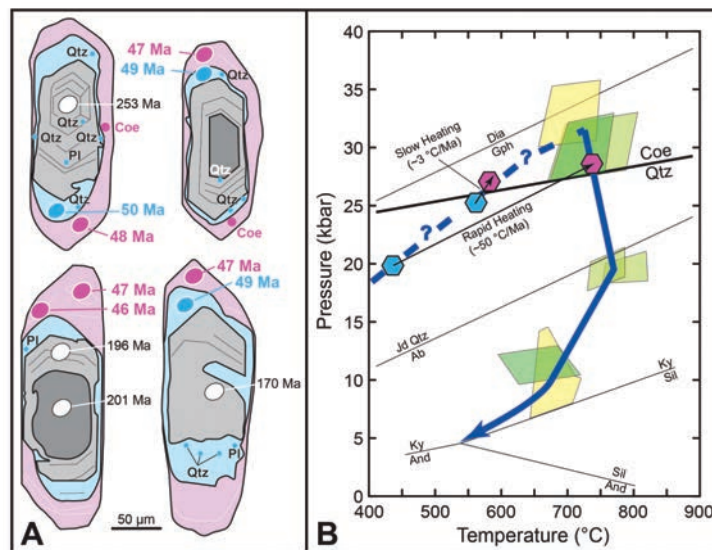


FIGURE 3. Mineral inclusions and ages in zircons from the Kaghan, Pakistan, UHP terrane. (a) Zircon domains with quartz inclusions average ~50 Ma, whereas domains with coesite inclusions average ~47 Ma, but not all dated zircon domains contain inclusions. From Kaneko et al. (2003). Thin lines illustrate cathodoluminescent bands. (b) P - T conditions and path. Although the prograde P - T path (dashed line) is not directly constrained, in principle the entrapment conditions for quartz (blue hexagon) and coesite (magenta hexagon) could be similar, implying slow tectonic processes (heating at ~3 °C/Ma), or disparate, implying rapid tectonic processes (heating at ~50 °C/Ma). Large boxes indicate P - T conditions from different studies (see summary of Kohn 2014b).

(i.e., $s = \Delta T_c / \Delta t$).

Dodson (1986) derived a simple and elegant form of the position-dependent closure temperature equation that applies to both types of calculations:

$$T_c(x) = \frac{E/R}{\ln \left[\frac{\epsilon R T_c^2 D_0 / a^2}{E \cdot s} \right] + 4S_2(x)} \quad (1)$$

where T_c and $T_c(x)$ are the bulk and position-dependent closure temperatures, E and D_0 are activation energy and pre-exponential term in an Arrhenius-type diffusion expression, R is the gas constant, a is the characteristic length scale of the mineral (e.g., radius of a spherical grain), s is the cooling rate, ϵ is the exponential of Euler's constant, $4S_2(x)$ is a tabulated position-dependent term, and x is the fractional distance from the mineral center. T_c and $T_c(x)$ are insensitive to s (which appears in the logarithm of the denominator), so a large change in s is required to balance a small change to T_c or $T_c(x)$.

To illustrate diffusion zoning principles, models were constructed based on Equation 1. Chemical zoning (Fig. 5c), $T_c(x)$, at a particular position was determined a priori from thermometric equations (e.g., garnet-biotite Fe-Mg exchange or Zr-in-rutile

thermometry; Fig. 5a), and s was adjusted for a specific pair of E and D_0 values until the correct $T_c(x)$ was achieved. Uncertainties in cooling rate can be calculated by propagating errors both in diffusion properties and calculated T_c . For E and D_0 , the value for E was perturbed by $+2\sigma$, the corresponding value for D_0 was calculated from experimental data (the two parameters are nearly perfectly correlated), and a new cooling rate determined to produce the same $T_c(x)$. Calculations were then repeated for $E-2\sigma$ and its corresponding D_0 . The difference in the cooling rates determined with the nominal values of E and D_0 vs. the perturbed values of E and D_0 provides a measure of the propagated uncertainty in s (Fig. 5c). The propagated analytical error in $T_c(x)$ ($\sim \pm 5$ °C for garnet-biotite; Kohn and Spear 1991b; as low as ± 2 °C for Zr-in-rutile) is typically smaller than propagated errors in E and D_0 and was ignored here.

For chronologic zoning (Fig. 5c), the ages at two positions were determined a priori, a "seed" value for s is assumed, and $T_c(x)$ values for diffusional reequilibration of the radiogenic daughter element were calculated using Equation 1 (Fig. 5b). An apparent cooling rate, s^* , was calculated from pairs of $T_c(x)$ and age (from the relation $s^* = \Delta T_c / \Delta t$) and substituted for s in Equation 1 iteratively until $s^* = s$. Again, values for E and D_0 may be varied within $\pm 2\sigma$ uncertainty, resulting in new $T_c(x)$

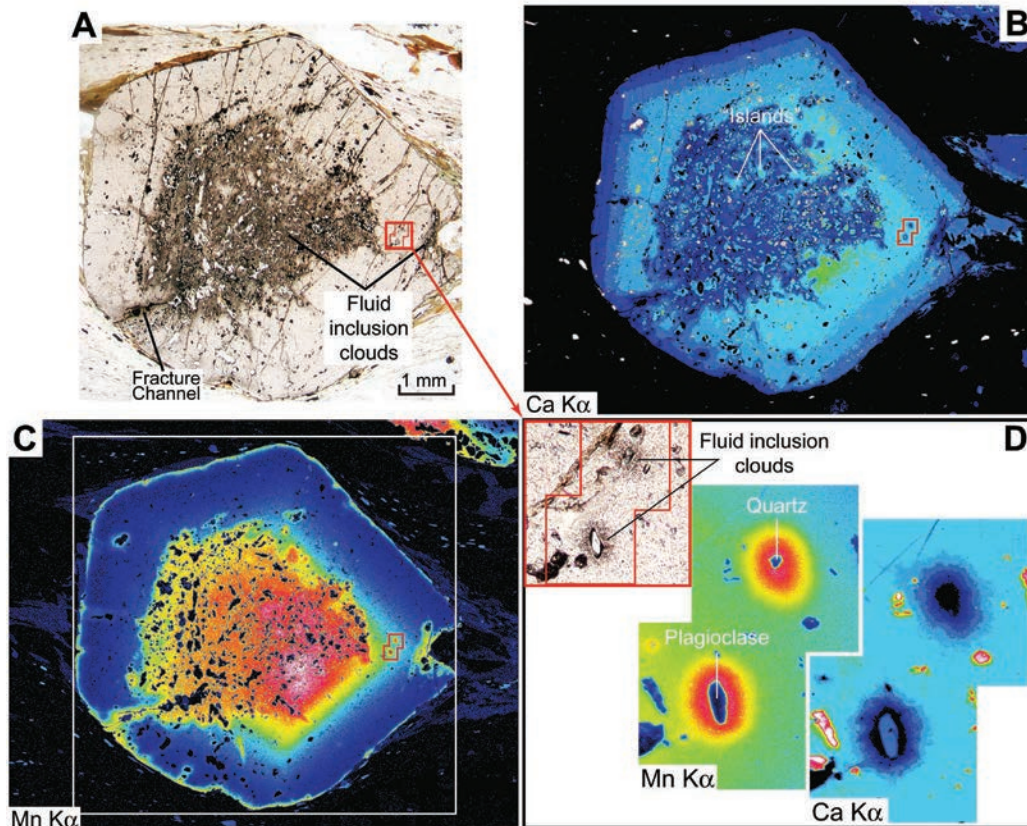


FIGURE 4. (a) Photomicrograph of garnet from Chile, showing dark clouds of fluid inclusions in garnet core and rim, and surrounding isolated mineral inclusions. These textures may reflect dissolution-precipitation (Putnis 2002), which can penetrate into garnet along fracture channels and alter chemistry (and presumably age of inclusions) even after entrapment. Red box shows region of high-resolution images in **d**. (b–c) X-ray maps of garnet showing chemical reequilibration (low Ca, high Mn) in replaced zones. White box in **c** shows region of photomicrograph (a). (d) High-resolution images of isolated inclusions of quartz and plagioclase showing fluid inclusion clouds and chemical reequilibration of garnet without obvious physical connections to matrix.

values and cooling rates (Fig. 5c). Chronologic error should also be propagated, specific to the isotopic and analytical system that is investigated, but was not considered here because it is quite sample-specific and error propagation is straightforward.

Uncertainties in diffusion properties propagate to considerably different uncertainties in cooling rates if chemical vs. chronologic zoning is modeled. As an example, uncertainties in diffusion parameters for Mg diffusion in garnet (Carlson 2006) were propagated numerically for a 1 mm radius grain cooling at 25 °C/Ma. Inversion of chemical zoning using Equation 1 yields a range of possible cooling rates between 15 and 45 °C/Ma, i.e., about a factor of 2 (Fig. 5c). Garnet is one of the best-studied minerals, so errors for other minerals are likely to be larger than calculated here. To make a direct comparison with chronologic zoning models, the same diffusion coefficients and their uncertainties were propagated assuming they pertained to a radiogenic

system. This results in a ~7% error in cooling rate, i.e., a nominal rate of 25 °C/Ma could range between 23 and 27 °C (Fig. 5c). Thus, inversion of chronologic zoning rather than chemical zoning is inherently more precise, as long as chronologic errors are not too large.

Calculated cooling rates tend to converge toward true cooling rates close to the physical edge of a mineral (Fig. 5c). But these calculations then become quite susceptible to slight growth or consumption, which moves the grain edge and changes the assumed length scale. For example, at 5 μm from the crystal edge, uncertainties in diffusion rates propagate to only ~30% error in calculated s when inverting chemical compositions (i.e., between 18 and 35 °C/Ma; Fig. 5c). Shifting the grain boundary inward by 5 μm, however, so that the present 5 μm position was originally 10 μm from the edge, increases calculated s by a factor of 4 (up to 100 °C/Ma). Dissolution shortens profiles and (erroneously) implies faster cooling rates, whereas growth lengthens profiles and (erroneously) implies slower cooling rates. Similar calculations for chronologic zoning suggest bias by a factor of ~2—still smaller than inversion of chemical zoning, but substantially larger than for a fixed boundary.

A final complication for inverting chemical profiles concerns how one models boundary compositions. For garnet, most models assume that its rim composition is controlled solely by retrograde exchange reactions (ReER; e.g., Fe-garnet + Mg-biotite = Mg-garnet + Fe-biotite). Garnet compositions at high temperatures, however, are more likely controlled by retrograde net-transfer reactions (ReNTR), which involve the net consumption or production of a mineral (e.g., garnet + K-feldspar + melt = sillimanite + biotite + plagioclase + quartz). Thermodynamic models demonstrate that garnet rim compositions are far more sensitive to temperature during operation of ReNTRs than ReERs (Spear 2004). So, even if the physical position of the garnet rim remains fixed, cooling rates that are calculated assuming that compositions are controlled by ReERs vs. ReNTRs can differ by 1–2 orders of magnitude (Spear 2004). Understanding the reaction history of the rock is clearly key for accurate modeling.

Examples

Garnets from a Himalayan gneiss in Sikkim, India, provide an example of chemically based geospeedometry (Ganguly et al. 2000; Fig. 6). Two different garnets show comparable zoning in Mg# toward their rims (Fig. 6a). Overall, this zoning is consistent with an average cooling rate of ~20 °C/Ma. In combination with a 1D thermal model, Ganguly et al. (2000) inferred accelerated cooling from 15 °C/Ma at 800 °C to ~200 °C/Ma at 450 °C. Chemical zoning in all four major components on the rims of garnets (Fig. 6b), however, suggest that the physical edge of the garnet might not have remained fixed and/or that rim compositions were affected by a ReNTR, not just Fe-Mg exchange. Slight resorption of the garnet rim, as suggested by a rimward increase in Mn, would lead to overestimated late-stage cooling rates, whereas operation of a ReNTR at high- T , such as melt crystallization, would lead to underestimated initial cooling rates. Thus, although a transition from slow cooling in the deep crust to rapid cooling in the shallow crust is completely consistent with petrologic observations, especially the formation of high- T , low- P assemblages (Ganguly et al. 2000), quantifying

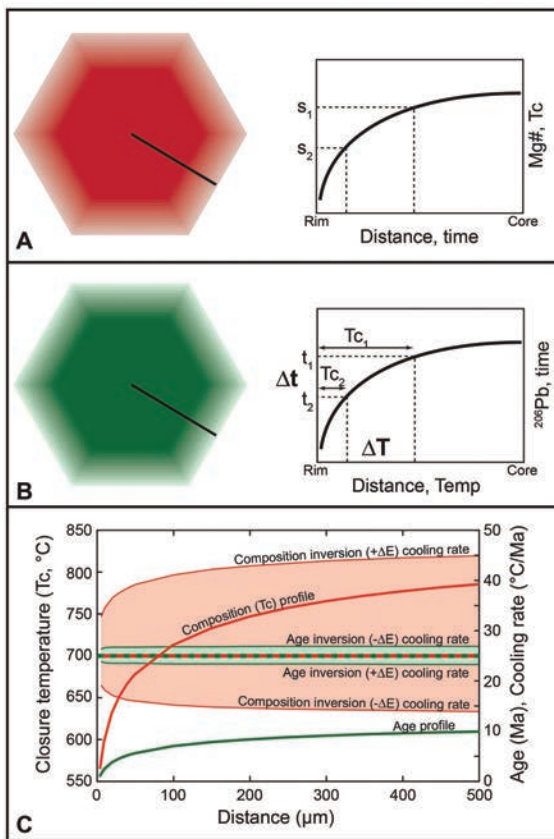


FIGURE 5. (a) Schematic of mineral with concentric chemical (temperature) zoning. The position of a composition, such as Mg#, is converted to closure temperature (T_c) and modeled in terms of cooling rate (s). (b) Schematic of mineral with concentric chronologic zoning. The position of an age (e.g., as represented by ^{206}Pb concentration for a fixed U content) is modeled in terms of closure temperature (T_c). Cooling rate (s) is determined from two T_c values and ages ($s = \Delta T/\Delta t$). (c) Uncertainties in retrieved cooling rate from chemical vs. chronologic zoning. Input cooling rate was 25 °C. Diffusion parameters are from Carlson (2006) for garnet. Uncertainties in activation energy (accounting for correlated changes to D_0) impose much larger errors in s using chemical rather than chronologic zoning.

cooling rates using chemical zoning may have large uncertainties.

Chronologically based geospeedometry was first attempted by using an ion microprobe to depth profile monazite from a Himalayan pegmatite in central Nepal (Grove and Harrison 1999). A decreasing age profile over the outer $\sim 1.5 \mu\text{m}$ of the crystal was modeled in terms of diffusive loss to infer rapidly decreasing cooling rates. Later experimental data on Pb diffusion in monazite (Cherniak et al. 2004; Gardés et al. 2007), however, imply that diffusive resetting is unlikely over even $0.1 \mu\text{m}$ distances. The decreasing age profile may instead reflect slight growth of monazite during cooling, which could be tested by analyzing other elements such as Y, Th, REE, etc., that respond to reactions. Analogously, although titanite U-Pb ages have traditionally been viewed as susceptible to diffusive resetting (Cherniak 1993), depth profiles from high-grade titanite from the central Himalaya indicate that Pb diffuses too slowly at $T \leq 800 \text{ }^\circ\text{C}$ to reset ages over $1 \mu\text{m}$ length scales (Kohn and Corrie 2011). Recent U-Pb data from rutile (Smye and Stockli 2014) are the best current candidate of diffusive chronologic closure profiles in accessory minerals (Fig. 7). A steadily decreasing age toward rutile rims, especially over the outer $\sim 10 \mu\text{m}$, is consistent with moderately rapid cooling between 185 and 175 Ma, followed by slower cooling to ~ 150 Ma.

CHEMICAL CORRELATION

Chemical correlation attempts to link chemistry with the rock's reaction history using geochemical and petrologic principles. In its simplest conceptual form, mineral compositions and the mass distributions of elements evolve during metamorphism, so by measuring the composition of whatever mineral (domain) is dated, an age can be linked to overall petrologic evolution, constraining the P - T condition of formation.

Monazite

Monazite is well studied, and research spans at least 15 yr (e.g., Pyle and Spear 1999, 2003; Pyle et al. 2001; Kohn et al. 2004, 2005; Kelly et al. 2006; Rubatto et al. 2013). In general, Th and Y contents of monazite decrease during solid-state metamorphic reactions, leading to Rayleigh-like depletions from core to rim (Fig. 8). For Y, decreases are linked to growth of garnet, which also depletes the rock in available Y (Fig. 8).

Our understanding of mineralogical distributions of Th is quite limited, so Th contents cannot be so simply linked to other minerals (except possibly allanite; Spear 2010). Regardless, Th contents in monazite are so high, any growth is likely to deplete the matrix and any later-grown monazite in Th. Interpretations beyond this level are restricted by relatively poor understanding of how other trace elements behave during metamorphism. For example, Corrie and Kohn (2008) were unable to mass balance many REE and concluded that grain boundary adsorption of REE might be important. Thus, even grain coarsening in the absence of prograde reactions might affect REE budgets and the growth and chemistry of monazite.

Partial melting changes compositional systematics dramatically because monazite is soluble in partial melts (Rapp et al. 1987; Montel 1993). The most important reaction for metasediments is the muscovite dehydration-melting reaction, which occurs at $T \sim 700 \text{ }^\circ\text{C}$ in typical bulk compositions (Spear et al. 1999). Upon melt crystallization, new monazite grows, commonly as high-Y and high-Th overgrowths on relict prograde grains (Pyle and Spear 2003; Kohn et al. 2004). These chemical principles allow identification of early-formed monazite (older high-Y and high-Th domains not on rims), monazite that formed in a late-prograde solid-state assemblage (low-Y and high-Th domains; $\leq \sim 700 \text{ }^\circ\text{C}$), and post-anatectic monazite (high-Y and high-Th overgrowths; $\leq 700 \text{ }^\circ\text{C}$). Peak metamorphic monazite in anatectic rocks is generally not expected because monazite should be dissolving.

Use of monazite chemistry for refining age interpretations is now widespread, and the following example from the Himalaya (Kohn et al. 2004, 2005) illustrates its power in the context of previous textural-only interpretations. In the Modi and Langtang areas of central Nepal, Kohn et al. (2004, 2005) and Corrie and Kohn (2011) studied several different structural levels (Fig. 9a) and identified several different compositionally and texturally distinct populations of monazite in each level (Fig. 9b): early prograde (high-Y and high-Th), late prograde (low-Y and low-Th), post-anatectic (high-Y and high-Th rims), and alteration (low-Y along cross-cutting fractures). A pre-Himalayan, high-U grain was also found. In anatectic rocks, late-prograde and post-anatectic compositions bracket the timing of melting and peak metamorphism, whereas in lower-grade rocks, late-prograde

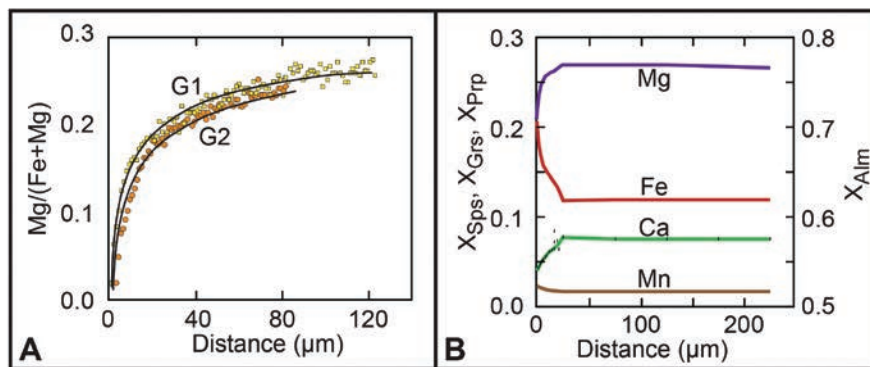


FIGURE 6. (a) Chemical zoning in garnet from Sikkim Himalaya, showing possible diffusion zoning in outer $\sim 100 \mu\text{m}$. This zoning can be modeled with an average cooling rate of $\sim 20 \text{ }^\circ\text{C/Ma}$. (b) Chemical zoning is present in all garnet components, suggesting that the edge position of the garnet has changed simultaneously with diffusion, complicating interpretation of temperature-time history. From Kohn (2013; based on Ganguly et al. 2000).

compositions limit the timing of peak metamorphism (Fig. 9b). Knowing peak metamorphic temperatures from thermobarometry (Kohn 2008) and the temperature of the muscovite dehydration-melting reaction, these data can be placed into a petrologically consistent thermal and tectonic model of orogenic wedge development (Fig. 9c). For example, crystallization of post-anatectic monazite from the highest structural level sampled along the Langtang transect at ~18 Ma occurred while the next structural level (the MCT sheet) was still heating to its peak (at ~16 Ma; between late-prograde and post-anatectic monazite ages). These data suggest thrust emplacement between 16 and 18 Ma, simultaneously cooling the upper plate and warming the lower plate. The same chronologic patterns continue down-section: the MCT sheet was cooling and crystallizing its melts at ~16 Ma while the next lower thrust sheet was still heating (early prograde monazite ages). This lower sheet had cooled through muscovite closure to Ar by at least 7.5 Ma, prior to peak metamorphism of the structurally lowest sheet. These patterns are expected for in-sequence growth of an orogenic wedge, but this example is the first clear documentation of this process in the Himalaya, and perhaps anywhere on Earth. Just as in the study of Catlos et al. (2001), a single rock or thrust sheet could exhibit a large range of monazite ages (e.g., 16 to 36 Ma in the MCT sheet at Langtang). Combination of ages with chemistry, however, links monazite ages with the rock's reaction history and broad regions of *P-T* space, which permits refined tectonic interpretations compared to textural-only interpretations.

The main complication in using monazite chemical correlation lies in its lack of compositional specificity. Although the temperature-time condition of melt crystallization can be determined with some confidence, the precise temperature of other dated domains can often be assigned only more generally. For example, in subsolidus rocks at Langtang the lowest-Y monazite domains were assigned to the peak of metamorphism, whereas they could have formed earlier. This ambiguity does not change the main tectonic interpretations in Nepal, but might elsewhere. And although a Y-in-monazite thermometer has been calibrated (Pyle et al. 2001), it requires compositional correlation with

several minerals. The ultimate correlation method would provide a direct quantitative measure of temperature or pressure from the dated domain itself.

Zircon

Chemical correlation methods have been proposed for zircon, particularly in reference to REE patterns (Rubatto 2002; Whitehouse and Platt 2003; Fig. 10). Fundamentally, interpretations focus on two features: the presence or absence of a Eu-anomaly, and the flatness of MREE-HREE patterns. Both methods emphasize mass balance. Europium warrants particular attention because, although the concepts appear founded in simple mass balance and petrologic principles, natural rocks may be more complex.

In most rocks, plagioclase takes up unusually high concentrations of Eu relative to other REE, so when plagioclase is stable, it should contain a disproportionate fraction of Eu, and all other minerals should have a negative Eu anomaly. As rocks transition to the eclogite facies, plagioclase breaks down to produce omphacite and garnet, which do not take up unusual amounts of Eu relative to other REE. Thus, plagioclase breakdown releases Eu back to the rock, flooding the rock with its reserve of Eu. Zircon formed in the plagioclase-stable field might be expected to have more pronounced negative Eu anomalies than zircon formed in the eclogite facies (Rubatto 2002).

While this mass balance argument appears plausible, it overlooks valence state—Eu taken up by plagioclase is divalent, whereas Eu taken up by zircon (and most other minerals) is trivalent. Therefore, breakdown of plagioclase and liberation of Eu^{2+} may have no impact on uptake of Eu^{3+} in zircon and consequently its Eu anomaly. One solution to this conundrum is to hypothesize that initial growth of metamorphic plagioclase nuclei takes up all available Eu^{2+} , and redox reactions cause partial conversion of residual Eu^{3+} to Eu^{2+} . Progressive growth of plagioclase and sequestration of Eu^{2+} ultimately removes virtually all Eu from the rock (similar to Mn uptake in garnet), and this Eu is now nearly all divalent. When plagioclase breaks down to form omphacite, a substantial amount of this Eu^{2+} is converted back to Eu^{3+} to maintain redox equilibrium, removing the Eu anomaly in zircon

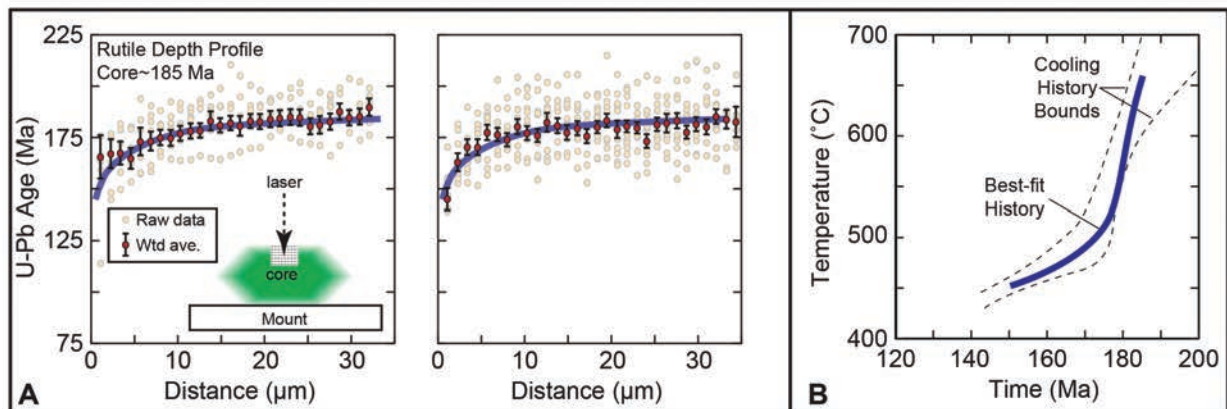


FIGURE 7. (a) Chronologic depth profiles in rutile, collected via LA-ICP-MS, for rocks from the Ivrea Zone, southern Alps, showing decreasing ages toward rim. Inset illustrates how laser is used to ablate natural crystal face. Raw data from Smye and Stockli (2014); weighted averages and minimum uncertainties recalculated using Eqs. 7 and 8a of Kohn and Spear 1991a). Blue line drawn through averaged data is the same in both panels. (b) Cooling history calculated assuming diffusion parameters of Cherniak (2000) and inversion technique of Ketchum (2005). From Smye and Stockli (2014).

and other minerals. If this hypothesis is correct, however, any process that allows plagioclase to equilibrate with the whole rock will allow its Eu^{2+} to replenish the Eu^{3+} reservoir and contribute to REE patterns in other minerals. For example, deformation-driven recrystallization or simple heating could enable Eu in plagioclase interiors to rejoin the reactive rock. The diffusion rate of Eu^{2+} in plagioclase is not known, but data for Sr suggest that diffusive equilibration may be possible at temperatures at or below $\sim 600^\circ\text{C}$ (Cherniak and Watson 1992, 1994). Therefore, the demise of a Eu anomaly in zircon, even if it is related to plagioclase equilibration, may reflect crossing a threshold temperature or strain rate.

Overall, MREE and HREE patterns in zircon are interpreted in the context of garnet growth. Prior to garnet formation, zircon REE patterns are assumed to have steep positive slopes (Rubatto 2002). Although the composition of a detrital zircon could be wholly unrelated to the host rock, depending on sediment sources, compilations of sediment and igneous compositions show relatively flat overall REE patterns (as normalized to chondrites; Fig. 10a). Because zircon strongly favors HREE to LREE compared to whole rocks (Sano et al. 2002), zircon compositions for average (meta-) sediments or mantle-sourced igneous rocks are predicted to exhibit steep REE patterns (Fig. 10a). Thus, it is not surprising that many detrital (usually igneous) zircon cores have steep REE patterns. Such a pattern is also generally predicted for metamorphic zircons that form in either metasedimentary or metaigneous rocks, as long as no other major sink of MREE and HREE is present (Fig. 10a). Why, then, do many metamorphic zircon overgrowths exhibit flat MREE-HREE patterns (Fig. 10b)? This chemical trend is consistent with growth of garnet because it preferentially takes up HREE.

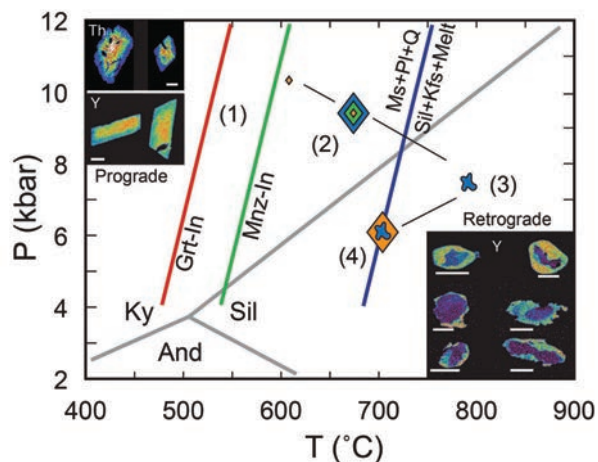


FIGURE 8. P - T diagram illustrating schematically the chemical evolution of monazite in the context of garnet growth and partial melting. Prograde monazite grows at the expense of allanite up to the muscovite dehydration-melting reaction (stages 1 and 2), with decreasing Y and Th due to Y and Th scavenging during monazite and garnet growth. Monazite dissolves during melting (stage 3), and during melt crystallization (stage 4) retrograde monazite with high Y and Th grows on relict cores. Upper left inset shows X-ray maps of prograde zonation in monazite from the southern Appalachians (Kohn and Malloy 2004). Lower right inset shows X-ray maps of retrograde chemical zoning in monazite from anatectic rocks of the central Himalaya (Kohn et al. 2005).

That is, garnet growth depletes the reactive matrix in HREE and causes HREE-depletion (flatter MREE-HREE patterns; Rubatto 2002; Whitehouse and Platt 2003), both in zircon (Fig. 10a) and progressively in garnet (Fig. 10b).

Knowing that a zircon grew with garnet (i.e., is metamorphic) can certainly be useful, but does that fact quantitatively limit P - T conditions? Recall that garnet is stable over an enormous region of P - T space (Fig. 10c), and a zircon could in principle form anytime from days to billions of years after garnet nucleation. Consequently, the conditions of zircon formation may not be significantly restricted. In fact, considering that metamorphic petrologists commonly study rocks that still contain (metastable) garnet crystals, a hypothetical zircon formed today, long after any metamorphic event and well outside the garnet stability field, would also be predicted to show a flat MREE-HREE pattern. Identifying that zircon formed in the presence of garnet surely does support the view that a zircon age is syn- to post-metamorphic, and such an age for a rock or terrane can be

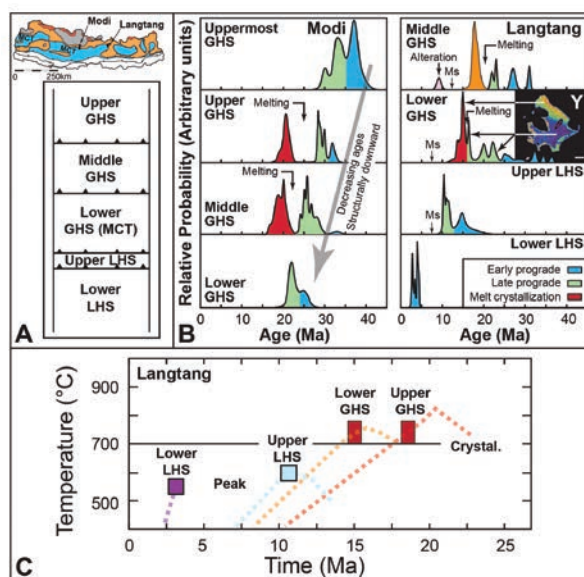


FIGURE 9. Age histograms of chemically characterized monazite domains from the central Himalaya [Kohn et al. 2004, 2005; muscovite $^{40}\text{Ar}/^{39}\text{Ar}$ ages (“Ms” with arrow) from Herman et al. 2010]. These data demonstrate steadily decreasing ages for any specific generation of monazite structurally downward, consistent with in-sequence thrusting. (a) Simplified structural section and geologic map of Nepal showing the locations of Modi and Langtang transects and the main lithotectonic units (Greater Himalayan Sequence, GHS = orange, Lesser Himalayan Sequence, LHS = blue, Tethyan Himalayan Sequence = gray, leucogranites = red). The Main Central Thrust (MCT) separates the Greater and Lesser Himalayan Sequences. (b) Monazite ages expressed as probability densities and color coded according to interpretation of chemistry. (c) Composite temperature-time histories in the context of possible thermal evolution (dashed lines) for rocks from the Langtang transect. “Peak” = estimated age of peak metamorphism for LHS rocks from youngest prograde monazite ages. “Crystal” = age of crystallization of in situ melts from age of post-anatectic monazite rims. Thermobarometry constrains peak temperatures (Kohn 2008). For each thrusting event, these data indicate simultaneous hanging-wall cooling during footwall heating.

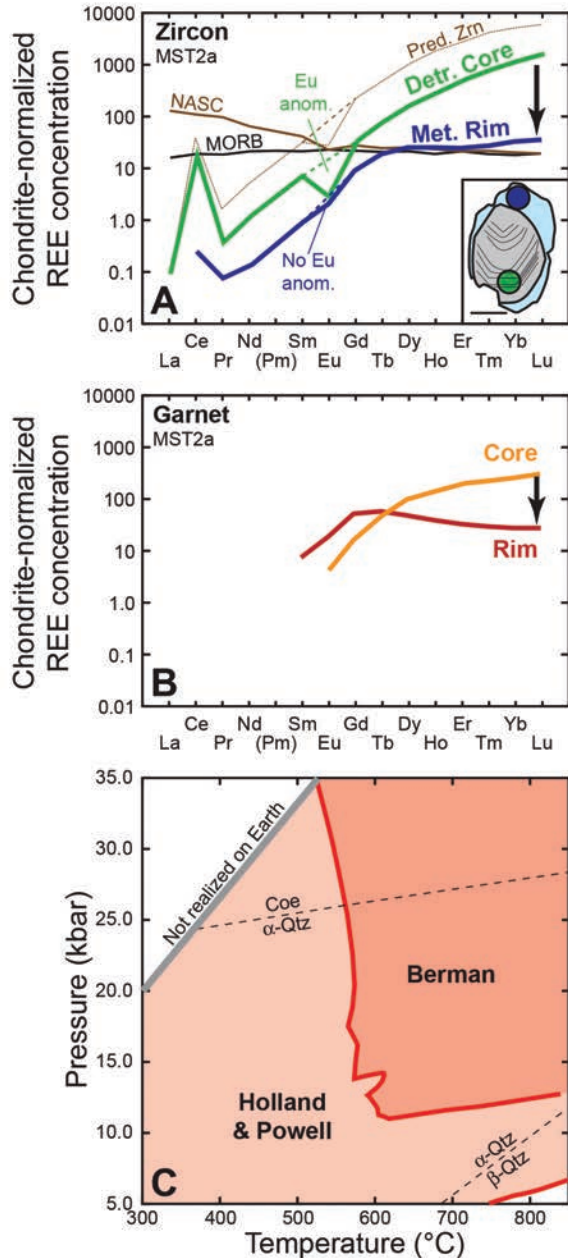


FIGURE 10. (a) Zircon and whole-rock REE patterns. NASC, MORB, and Pred. Zm are the North American Shale Composite (Gromet et al. 1984), Mid-Ocean Ridge Basalt (Arevalo and McDonough 2010), and zircon that would be in equilibrium with NASC assuming zircon–whole-rock partition coefficients of Sano et al. (2002). “Eu anom.” = europium anomaly. “Detr. Core” and “Met. Rim” show measured detrital core and metamorphic rim for zircon from eclogite-facies rock, Italy (Rubatto 2002). Inset shows sketch of zircon analyzed; thin lines represent oscillations evident from cathodoluminescence imaging. Scale bar is 50 μm . (b) REE patterns for garnet from the same eclogite-facies rock, showing evolution from steep to flat HREE pattern from core to rim (Rubatto 2002). (c) Prediction of garnet stability field in metabasalt for two commonly used thermodynamic databases (Berman 1988, modified in Berman and Aranovich 1996; Holland and Powell 1998; see also Kohn et al. 2015), illustrating large field of garnet stability. Fields completely overlap in the area labeled “Berman.”

tectonically useful. But clearer delineation of the P - T conditions of zircon formation and placement of the age in a coherent petrologic context requires additional, more detailed, petrology and thermobarometry.

DIRECT COMBINED THERMOMETRY AND GEOCHRONOLOGY

The latest research seeks to link ages directly with temperature through simultaneous geochronology and trace element thermometry in single microanalytical spots. Zircon, titanite, and rutile are all amenable to geochronologic and thermometric microanalysis, exploiting the U-Pb system and the experimentally calibrated Ti-in-zircon, Zr-in-titanite, and Zr-in-rutile thermometers (Watson et al. 2006; Tomkins et al. 2007; Hayden et al. 2008). Applications depend on relative diffusivities of Pb vs. thermometric trace elements. Diffusion of Pb and Ti in zircon is extremely slow (Cherniak and Watson 2001, 2007), so zircon domains should faithfully preserve both their Ti-in-zircon temperatures and U-Pb ages over virtually all metamorphic conditions. Titanite’s Zr diffusivity is sufficiently slow that it should retain its Zr temperature up to at least 750 °C (Cherniak 2006) and Himalayan titanite data (Kohn and Corrie 2011) show no evidence of near-rim ($\leq 2 \mu\text{m}$) diffusive reequilibration of Zr at peak temperatures of 775 °C. Although experiments suggest relatively fast Pb diffusivities in titanite, with a typical T_c of ca. 600 °C (Cherniak 1993), recent chronologic data can be explained only if Pb diffusion is extremely slow, with a T_c of at least ~ 800 °C. For example, depth profiling of titanite crystal faces from ~ 775 °C rocks in the Himalaya cannot be reconciled with models of diffusive Pb loss (Kohn and Corrie 2011), and titanite cores in rocks from the Western Gneiss Region retain protolith ages of ca. 1 Ga despite Caledonian UHP metamorphism that culminated in temperatures of ~ 780 °C (Spencer et al. 2013). If Pb diffusivities were as fast as indicated experimentally, diffusion profiles should be ubiquitous in such high- T grains, and older ages should be eradicated. Thus, although experimentally and empirically determined diffusivities for other elements and minerals are commonly compatible, experimental results for Pb diffusion in titanite appear exceptionally incompatible with nature. Rutile has faster diffusivities for Pb and Zr with typical T_c values of 600–650 °C (Cherniak 2000; Vry and Baker 2006; Cherniak et al. 2007). Thus, rutile inclusions might be used to constrain prograde temperature-time points, whereas matrix grains in higher- T rocks could be modeled in terms of diffusive loss (Smye and Stockli 2014).

Titanite

Investigation of calc-silicate titanite crystals in the Himalaya (Kohn and Corrie 2011; Fig. 11a) illustrates how thermometry and chronology can be combined to improve understanding of a rock’s thermal history. Samples from the anatectic Greater Himalayan Sequence in the Modi region of central Nepal reached peak temperatures of ~ 775 °C (Corrie and Kohn 2011). Both depth profiling and spot analysis of grains in thin section showed significant differences in temperature (Zr content) and U-Pb age that were inconsistent with diffusive resetting. By measuring both temperature and age for each spot, these data suggest slow heating from ~ 700 to ~ 780 °C between ~ 35 and ~ 25 Ma, followed

by slight cooling to ~ 765 °C by ~ 21 Ma (Fig. 11a). Rapid cooling commenced immediately afterward, as indicated regionally by monazite crystallization from in situ anatectic melts at 20 ± 2 Ma and muscovite $^{40}\text{Ar}/^{39}\text{Ar}$ ages of 14–15 Ma (Godin et al. 2006). If diffusion did not bias these observations, they require much more protracted heating than commonly considered for the Himalaya. This result is important for crustal geodynamics because it implies that hot weak zones can exist in the crust for millions of years without nucleating or focusing shear structures (Kohn and Corrie 2011).

A complementary study of titanite from the Western Gneiss Region (Spencer et al. 2013) suggests that regional temperature-time histories can be inferred through microanalysis of this mineral in multiple rocks (Fig. 11b). Spencer et al. (2013) combined numerous trace element and U-Pb microanalyses of different titanite grains from individual rocks to infer each rock's average temperature and age. This approach assumes data for a sample represent a single population of grains, which is appropriate for most of their rocks. Although less elegant than a crystal-domain-specific approach, combining data improves

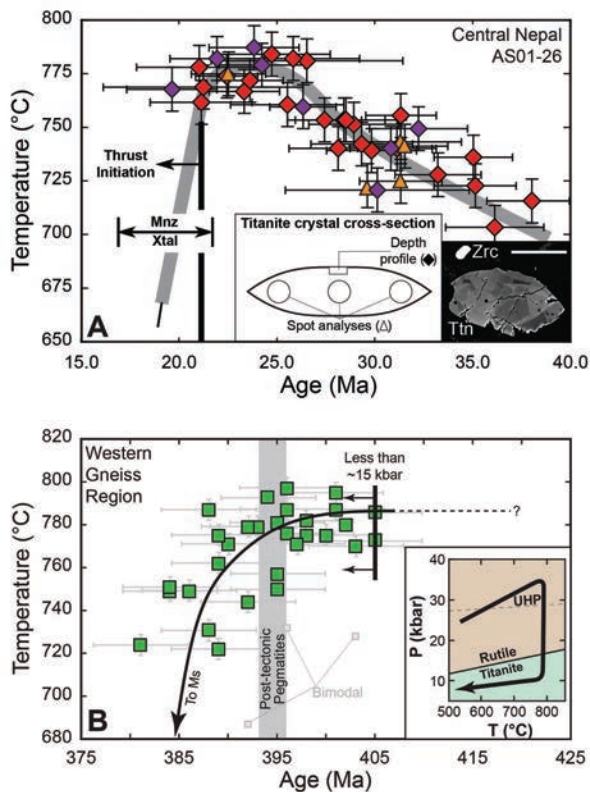


FIGURE 11. Temperature-time histories from combined U-Pb dating and Zr-thermometry of titanite. (a) Different domains from titanite in a single rock from the Greater Himalayan Sequence, Modi region, central Nepal. From Kohn and Corrie (2011). Insets show analytical methods (depth profiling vs. spot analyses) and domain-style compositional heterogeneity in backscattered electron image of titanite. Scale bar is 100 μm . (b) Titanite data from multiple rocks in the Western Gneiss Region UHP terrane, Norway (data from Spencer et al. 2013). Inset shows titanite stability field for typical Western Gneiss Region gneisses (Spencer et al. 2013). Modified from Kohn et al. (2015).

chronologic resolution, which can be necessary in older orogens where individual spot analyses carry large age uncertainty. For example, in the Himalaya a 5–10% error may be tolerable (only ± 1 –3 Ma), whereas in the Paleozoic, the same relative error translates to much larger absolute uncertainties (± 20 –40 Ma), which can impede tectonic interpretations. Some datapoints for Western Gneiss Region titanites are obvious outliers and inspection of raw data indicates they do not conform to a single population, but exhibit a bimodal distribution of Zr contents or ages; these are ignored in the present discussion. Overall, the titanite data set suggests high- T as early as 405 Ma, followed by rapid cooling to muscovite closure by 380–385 Ma (Young et al. 2011; Fig. 11b). Titanite is unstable above $P \sim 15$ kbar in these rocks (Spencer et al. 2013; inset, Fig. 11b), so, unlike in the Himalayan calc-silicates, titanite illuminates the late-stage exhumation and thermal history, not early-stage processes. Models for petrologic evolution of UHP rocks in western Norway imply that temperatures must have been similarly high near maximum pressures, implying a flat earlier temperature-time history (dashed line, Fig. 11b). Until Spencer et al.'s work, views on the age of high-pressure (HP) and UHP metamorphism had ranged from ~ 395 to ~ 425 Ma (e.g. see summary of Kylander-Clark et al. 2009). Because titanite is a late-stage, relatively low- P mineral, however, the titanite data demand HP and UHP metamorphism before ~ 405 Ma.

Zircon

Because of slow intracrystalline diffusivities, zircon is an obvious target for combined thermometry and geochronology, but relatively little systematic work has yet attempted to construct temperature-time histories or compare with other independent data. Zircons from Himalayan leucogranites and migmatites in the Sikkim region of India (between Nepal and Bhutan) are worth considering because recent studies provide a rich data set (Kellett et al. 2013; Rubatto et al. 2013), and because such data potentially elucidate interactions among melt formation, thrust movement, and lower crustal flow. The following discussion is somewhat complex, but illustrates the interpretability of zircon metamorphic chronology.

Several factors in the context of host-rock T - t paths impact expected temperatures recorded by these anatectic magmas and their zircons. (1) Inherited zircons are common, so the melts were always saturated in zircon. This permits additional application of whole-rock zircon-saturation thermometry (Watson and Harrison 1983; Boehnke et al. 2013) as a cross-check to Ti-in-zircon temperatures. However, zircon inheritance implies that calculated zircon-saturation temperatures are maxima. (2) Many in situ and cross-cutting melts are thought to have formed via muscovite dehydration-melting (Inger and Harris 1992; Harris and Massey 1994), which occurs at ~ 700 °C in plagioclase-bearing rocks (Spear et al. 1999; dry solidus, Fig. 12a). Without other consideration, this implies that most Ti-in-zircon and zircon-saturation temperatures should be at least 700 °C. (3) A low-temperature zircon cannot crystallize in a high-temperature host-rock, so the host-rock T - t path limits the region of T - t space available to Ti-in-zircon temperatures (Permissible vs. Forbidden Zones, Fig. 12a). For example, for the hypothetical T - t curve in Figure 12a, a 700 °C zircon could crystallize only ≥ 34 or ≤ 13 Ma, not near the peak of metamorphism. (4) If host-rock temperatures increase after

muscovite dehydration-melting, any melts present in the host-rock should continue to dissolve zircon and consequently record zircon saturation temperatures greater than or equal to the peak

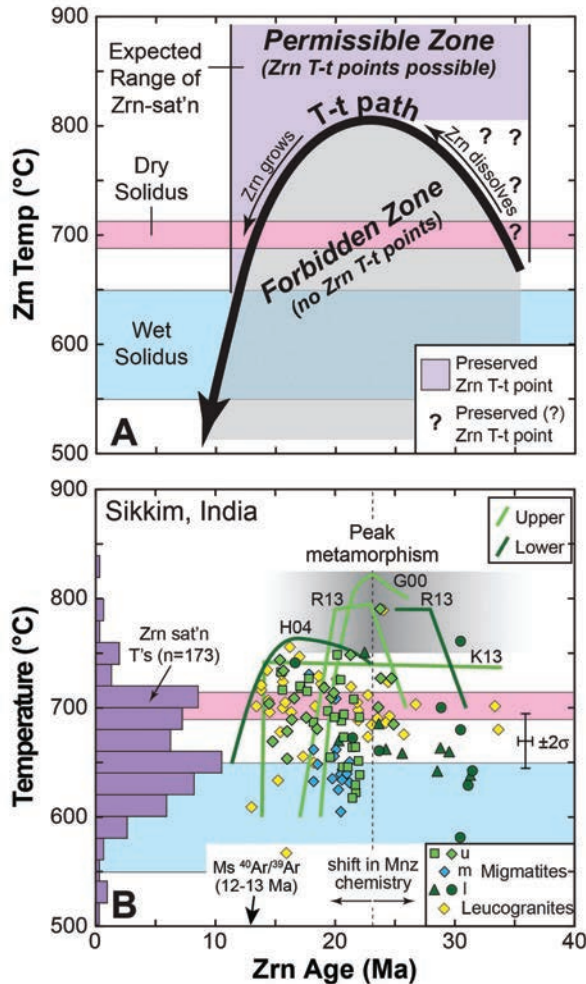


FIGURE 12. (a) Schematic of expected Ti-in-Zrn and Zrn-saturation temperatures for migmatitic melts and leucogranites relative to $T-t$ history of host rocks. Zircons should record temperatures at least as high as the host-rock temperature (Permissible Zone), not below the host-rock $T-t$ curve (Forbidden Zone). Early formed lower- T zircons (e.g., ~750 °C at 35 Ma) may not survive later heating (question marks in Permissible zone). The dry solidus corresponds to the temperature of the muscovite dehydration-melting reaction. The wet solidus accounts for possible low- P crystallization and presence of high B content. (b) Temperature-time points from combined zircon U-Pb dating and Ti-thermometry for Sikkim, India, region of the east-central Himalaya (data sources in Kohn 2014b). Ti-in-zircon thermometry suggests $T \leq \sim 700$ °C since 35 Ma and fall well below estimated peak metamorphic T_s , but are consistent with zircon-saturation thermometry of leucogranites and migmatitic segregations across the Himalaya (histogram; modified from Kohn 2014b, to include data from Scaillet et al. 1990; Guo and Wilson 2012; Thöni et al. 2012; Zeng et al. 2012; Carosi et al. 2013; and Liu et al. 2014). A shift in monazite chemistry at 20–25 Ma (Rubatto et al. 2013) may indicate a transition to regional cooling. Proposed $T-t$ curves are from Ganguly et al. (2000; G00; assuming peak age of 23 Ma), Harris et al. (2004; H04), Rubatto et al. (2013; R13), and Kellett et al. (2013; K13).

temperature. Magmas formed after the peak of metamorphism might record lower temperatures. (5) Himalayan leucogranites are famous for high boron contents (Searle and Fryer 1986), which lowers the solidus by 50–100 °C (Chorlton and Martin 1978). Fractional crystallization or concentration of H_2O into melts might also lead to solidus temperatures closer to the wet solidus. If so, magmatic zircons might crystallize at even lower temperatures, perhaps as low as 550 °C, but again only very early or very late in the metamorphic evolution (schematically ≥ 35 or ≤ 10 Ma, Fig. 12a).

Two main chronologic data sets have been collected from leucogranites and migmatites in the Sikkim region (Kellett et al. 2013; Rubatto et al. 2013). Petrologic studies there consistently infer high host-rock temperatures that persisted during quasi-isothermal exhumation from ~10 to ~4 kbar (Neogi et al. 1998; Ganguly et al. 2000; Harris et al. 2004; Rubatto et al. 2013). Fit to thermal models, these paths imply temperature-time histories that peak at ~800 °C and cool rapidly thereafter (Fig. 12b). Different studies infer different paths (in part depending on structural level; green lines, Fig. 12b), but all broadly show rapid cooling around 15–20 Ma and high temperatures at 20–25 Ma. The timing of peak metamorphic conditions is based on changes to monazite chemistry in dated grains (Rubatto et al. 2013), dated peritectic garnets (Harris et al. 2004), and geochronology of high-grade rocks in the region (e.g., Li et al. 2003; Cottle et al. 2009b; Corrie et al. 2010). Thus, we expect that Ti-in-zircon temperatures should fall above specific proposed $T-t$ curves, with an absence of low- T ages between ~15 and ~25 Ma.

Nearly all zircon data strikingly contradict expectations, as nearly all fall below proposed $T-t$ histories for host-rocks, and are well below 800 °C between 15 and 25 Ma. The low Ti-in-zircon temperatures, however, are completely consistent with zircon-saturation temperatures inferred from a synthesis of Himalayan leucogranites (Kohn 2013; Fig. 12b). Thus the data create a major interpretational conflict. The zircon data are internally consistent—Ti-in-zircon and zircon-saturation temperatures are consistently low and make sense in the context of low solidus temperatures expected for boron-rich melts. However, these data imply that temperatures must have been less than 600–650 °C since 25–30 Ma, whereas petrologic and alternate geochronologic data indicate otherwise. Apparently one (or more) of three observations must be discounted: the petrologic interpretations of high temperatures, the timing of peak metamorphism, or the combined Ti-in-zircon and zircon-saturation temperatures.

Several studies now argue that the same structural levels elsewhere in the Himalaya attained temperatures commensurate with partial melting by ~35 Ma (Kohn and Corrie 2011; Imayama et al. 2012; Thöni et al. 2012; Rubatto et al. 2013; Wang et al. 2013). Although many ages >25 Ma likely reflect subsolidus prograde metamorphism (Kohn et al. 2004, 2005; Cottle et al. 2009a; Langille et al. 2012; Stübner et al. 2014), possibly the high-temperature assemblages at Sikkim were produced prior to ~30 Ma, disconnecting peak metamorphism from zircon and leucogranite crystallization. That is, the “Forbidden Zone” (Fig. 12a) might predate the zircon ages (Fig. 12b). Alternatively, high- T (low- P) assemblages at Sikkim might reflect local heating associated with intrusions, so that although local temperatures were high (briefly), regional temperatures were low, causing

sequential crystallization of melts. The correspondence between Ti-in-zircon and zircon-saturation temperatures argues against thermometer inaccuracies. Further research integrating petrology with geochronology is needed to resolve this issue.

DISCUSSION: PROS AND CONS

Clearly, methods of linking chronologic and petrologic data have evolved substantially over the last 20 yr. This trend is illustrated by my own microanalytical research, which progressed from texturally based studies (Catlos et al. 2001; Kohn et al. 2001), to petrologically and chronologically linked research (Kohn et al. 2004, 2005; Corrie and Kohn 2011), to direct chronologic and thermometric analysis (Kohn and Corrie 2011). Each approach brings advantages and disadvantages, and every method will work well in some rocks. Inclusions, if unaltered after entrapment, surely imply that the host mineral crystallized during or after formation of the inclusion mineral, so the age of the inclusion either dates or predates that zone in the host mineral. This simple concept has substantial power, for example in the identification of early UHP metamorphism in the Himalaya (Kaneko et al. 2003; Fig. 3). Nonetheless, a little geochemistry goes a long way toward improving interpretations. The composition of monazite, particularly Y and Th contents, distinguishes different generation domains and allows refined tectonic interpretations (Kohn 2008; Fig. 9). Although simultaneous chronology and thermometry has particular power, this approach is not feasible for many minerals or rocks. For example, monazite is chronologically invaluable, but has no simple trace element thermometer (the Pyle et al. 2001, Y-in-monazite thermometer requires compositional correlation with several other minerals), so studies must continue to emphasize chemistry in the context of models. In contrast, rutile's low U content makes chronology difficult, but high Zr makes thermometry comparatively easy. The lingering discrepancies in the Himalaya between petrologic temperatures and regional geochronology vs. Ti-in-zircon and zircon-saturation temperatures are particularly worrying. Overall, data that combine geochronology and thermometry are as yet too sparse to pronounce judgment, but the potential payoffs are substantial, and further exploration of the systematics in different minerals is needed.

NEW DIRECTIONS AND IMPLICATIONS

Future work can and should expand the use of geochemically based (petrochronologic) methods. For example, relatively routine depth-profiling methods for trace elements open a vast array of potential mineral-element systems amenable to the inversion of chemical diffusion profiles to infer cooling rates. Further exploration of this method might tax the patience of experimentalists, as petrologists request data on an ever-increasing list of elements and minerals. Ultimately, however, this work will refine our understanding of diffusion rates and element mobility during metamorphism, and steadily reduce cooling rate uncertainties. Similarly, new measurements of ever-larger arrays of trace elements in chronologically useful minerals like monazite will help identify *P-T* conditions of formation more precisely. Besides these obvious directions, two other potential realms of inquiry are considered—modeling and thermobarometry. The former is a necessary complement to geochemical methods

now in practice. The latter represents an entirely new direction of research and promises a new era in textural correlation studies by quantifying pressures and temperatures of inclusion entrapment.

Modeling

Trace element abundances and distributions among metamorphic minerals fundamentally control accessory mineral stability and growth. In contrast to numerous models for common rock-forming silicates and oxides, fewer models address accessory minerals. A few studies have tackled monazite (Janots et al. 2007; Kelsey et al. 2008; Spear 2010; Spear and Pyle 2010), emphasizing Y and REE, but the difficulties of accounting for individual trace elements to model REE patterns are substantial, and quantitative attempts are as yet lacking. At least one empirical study has implicated grain boundaries as a reservoir for REE (Corrie and Kohn 2008), which further complicates modeling. Zircon is more amenable to theoretical modeling because, to a first order, Zr is the only trace element that requires mass balancing. Models have now been constructed for metapelites (Kelsey et al. 2008; Kelsey and Powell 2011; Yakymchuk and Brown 2014; Kohn et al. 2015) and metabasites (Kohn et al. 2015), and results provide broad recommendations for interpreting zircon ages. Models from Kohn et al. (2015) are discussed here because they consider Zr partitioning among metamorphic minerals more comprehensively and extend to higher pressures relevant to UHP terranes (35, rather than 12–20 kbar in other studies).

In Kohn et al.'s models, modes and Zr contents of minerals were monitored along three representative *P-T* paths (Fig. 13). For metabasite models (Figs. 13a and 13b), two different thermochemical databases were used (Berman 1988 and Berman and Aranovich 1996; Holland and Powell 1998). For metapelites (Figs. 13c and 13d), the Holland and Powell (1998) thermochemical database was used. Each model shows essentially the same basic pattern—the matrix takes up increasing amounts of Zr during prograde metamorphism, particularly rutile in metabasites and melts in metapelites. Thus the mode of zircon decreases until the maximum temperature (in metabasites) or maximum melt content (in metapelites) is reached (Figs. 13a–13d; see also Kelsey and Powell 2011; Yakymchuk and Brown 2014). Depending on the *P-T* path, the reduction in zircon mode can be moderate (~10%) to large (~50%). During exhumation and cooling, Zr is returned to the matrix to form new zircon, especially as melts crystallize and low-Zr ilmenite or titanite replaces high-Zr rutile. These results suggest that metamorphic zircon should mainly record the later stages of metamorphism, not peak or prograde processes. Obviously zircon might actually grow on the prograde path because of other processes that are not included in models, such as dissolution of metamict or micro-grains elsewhere in a rock with reprecipitation onto relict grains (Dempster et al. 2008). For example, the older quartz-bearing domains in the Kaneko et al. (2003) study might represent such a case. In general, such processes simply redistribute existing zircon, however, and most metamorphic zircon is predicted to form relatively late.

Zircon ages from the Western Gneiss Region of Norway (Fig. 13e) generally conform to model predictions. Titanite ages provide unequivocal evidence for the timing of late-stage exhumation and cooling, certainly below ~15 kbar (Spencer et al. 2013; Figs. 11b and 13c). Metamorphic zircon ages (Car-

swell et al. 2003; Root et al. 2004; Young et al. 2007; Krogh et al. 2011; Gordon et al. 2013; Beckman et al. 2014) show that most (~70%) overlap titanite ages (Fig. 13e). Like titanite, zircon must have formed at relatively low-*P* late in the region's metamorphic evolution. These results are consistent with Sm-Nd garnet ages, which also overlap zircon ages (Fig. 13e). Diffusivities of Nd in garnet are sufficiently fast that ages in these rocks should dominantly reflect closure at temperatures of 700–800 °C (Burton et al. 1995; Ganguly et al. 1998), depending on grain size and cooling rate, and rarely reflect maximum pressures. Some zircon ages overlap Lu-Hf garnet ages (Kylander-Clark et al. 2009) and a Th-Pb age of a monazite inclusion in garnet

(Terry et al. 2000; Fig. 13e). These might reflect either prograde metamorphism or maximum pressures, but only a minority of zircon ages falls within this range. Overall, these data reinforce the conclusion that metamorphic zircon should commonly be a late-crystallizing phase.

The general success of modeling zircon notwithstanding, inclusions of prograde metamorphic minerals in zircons demonstrate that mass balance and element partitioning cannot solely control mineral growth. Future work must identify what other factors control formation of accessory minerals. For minerals like monazite, apatite, and allanite, a much better understanding of REE, Th, P, and F is needed. Models will require substantial

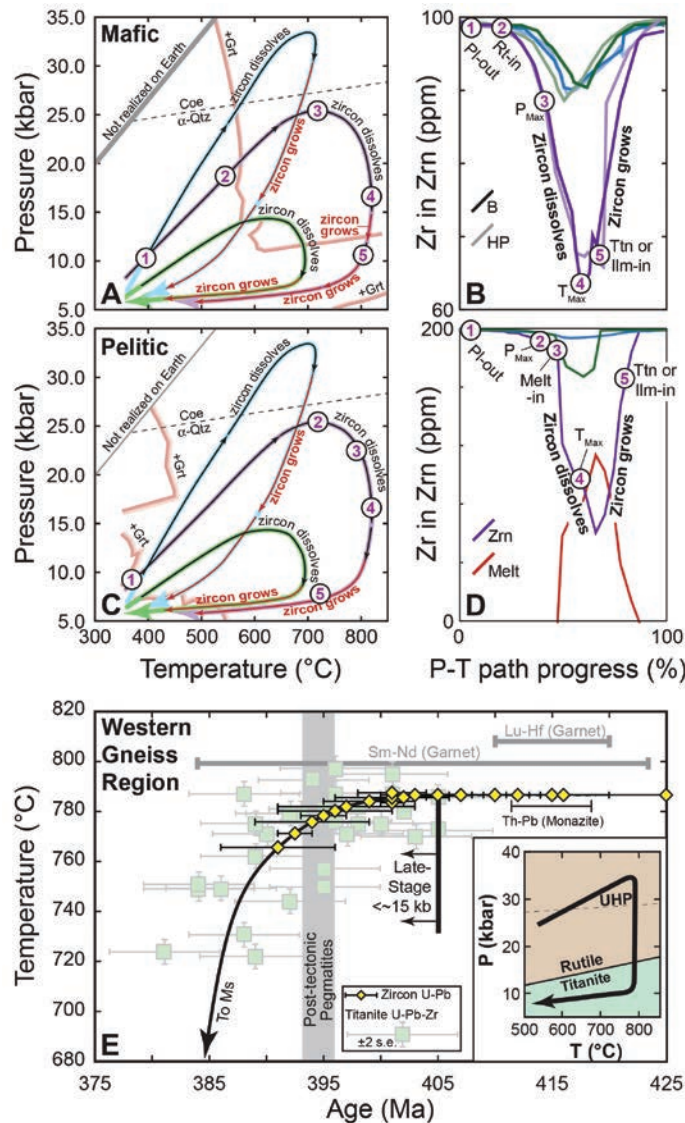


FIGURE 13. (a–d) Zirconium mass-balance models modified from Kohn et al. (2015) showing that zircon mode should decrease during prograde metamorphism and increase during retrograde cooling. Points 1–5 reflect important mineralogical changes. (a–b) Mafic models. “+ Grt” = garnet stability fields predicted by the thermodynamic database of Holland and Powell (1998) (“HP”) vs. the thermodynamic database of Berman (1988) and Berman and Aranovich (1996) (“B”). Rutile strongly controls amount of Zr available to zircon. (c–d) Pelitic model based on the Holland and Powell (1998) thermodynamic model. Melt strongly controls amount of Zr available to zircon. (e) Zircon ages from Western Gneiss Region superimposed on *T-t* path from titanite, showing that most ages are late-stage (post-UHP). Regional chronologic constraints from garnet (see summary of Kylander-Clark et al. 2009) and monazite (Terry et al. 2000) shown for reference. Modified from Kohn et al. (2015).

prior effort to constrain partitioning among metamorphic minerals and identify reservoirs of trace elements, as well as constrain the kinetics of trace element movement in metamorphic rocks. Numerous reports of compositional oscillations, sector zoning, and patchy zoning for trace elements in garnet (e.g., Spear and Kohn 1996; Chernoff and Carlson 1999; Yang and Rivers 2001, 2002; Lapen et al. 2003; Kohn 2004, 2013; Vielzeuf et al. 2005) suggest that kinetics plays a major role and that development of fully quantitative models will prove challenging.

Thermoba-Raman-try

Although Raman spectroscopy on mineral inclusions has been applied for about 15 yr to recover pressures of original entrapment (Israeli et al. 1999; Sobolev et al. 2000), concurrent and subsequent theoretical developments (Zhang 1998; Guiraud and Powell 2006; Kohn 2014a; Kouketsu et al. 2014) and applications to common crustal rocks (Enami et al. 2007; Ashley et al. 2014; Kouketsu et al. 2014; Spear et al. 2014) have recently promoted this technique to the leading edge of thermobarometric research. At the time of inclusion entrapment, no differential pressure occurs between inclusion and host mineral. Because host and inclusion have different thermal expansivities and compressibilities, however, a differential pressure develops during exhumation and cooling. As originally developed by Rosenfeld and Chase (1961) the line of permissible entrapment conditions of an inclusion can be calculated (subject to certain geometric constraints) based on the present-day magnitude of the pressure on the inclusion, the volume equation of state of the host and inclusion, and the shear modulus of the host. Many host-inclusion pairs are quite pressure-sensitive (e.g., quartz-in-garnet, “QuiG”), whereas others are decidedly temperature-sensitive (e.g., zircon-in-garnet, “ZiG”; Fig. 14a).

Raman confocal microspectroscopy plays a key role by measuring band position shifts of in situ inclusions relative to standard state spectra. Raman band positions depend on pressure,

and that dependence has been calibrated for numerous common minerals. Thus, Raman band shifts for inclusions can be inverted to infer present-day inclusion pressures, and the present-day pressures can be inverted using standard calibrations to identify entrapment conditions (e.g., Kohn 2014a; Figs. 14a and 14b). This combination of the use of Raman spectroscopy in thermobarometric endeavors gives rise to the term “thermoba-Raman-try” (Kohn 2014a). The analytical uncertainties on retrieved P - T conditions are encouragingly small: only a few hundred bars for quartz inclusions in numerous minerals (garnet, clinopyroxene, epidote, ilmenite, kyanite, lawsonite, magnetite, staurolite, titanite, tourmaline, rutile, and zircon), and a few tens of degrees for zircon in several minerals (garnet, clinopyroxene, epidote, kyanite, and titanite; Kohn 2014a; Figs. 14a and 14b). Because analysis is wholly non-destructive, even these acceptably small errors can be reduced through multiple repeat analyses of the same inclusion.

An example from the Himalaya illustrates the correspondence that is possible between thermoba-Raman-try and conventional thermobarometry. Corrie and Kohn (2011) conducted a regional study of metamorphic rocks in the Modi region of central Nepal. One rock from the Greater Himalayan Sequence crystallized at an inferred peak P - T condition of ~ 750 °C and 11–12 kbar (Fig. 14a). Quartz and zircon inclusions occur near the edge of garnets from this rock, and thermoba-Raman-try on them intersects at a P - T condition of about 11 kbar and 725 °C, close to, albeit slightly lower than the conventional thermobarometric estimate. The difference is within analytical error, but the Raman-based estimate could also reflect either a P - T condition prior to the metamorphic peak or slight reequilibration during exhumation and cooling.

Further exploration of thermoba-Raman-try is needed to identify its practical strengths and weaknesses, but published examples already predict a new era for P - T studies. Although inference of entrapment pressures using coesite inclusions is doomed for most rocks because of partial transition to quartz

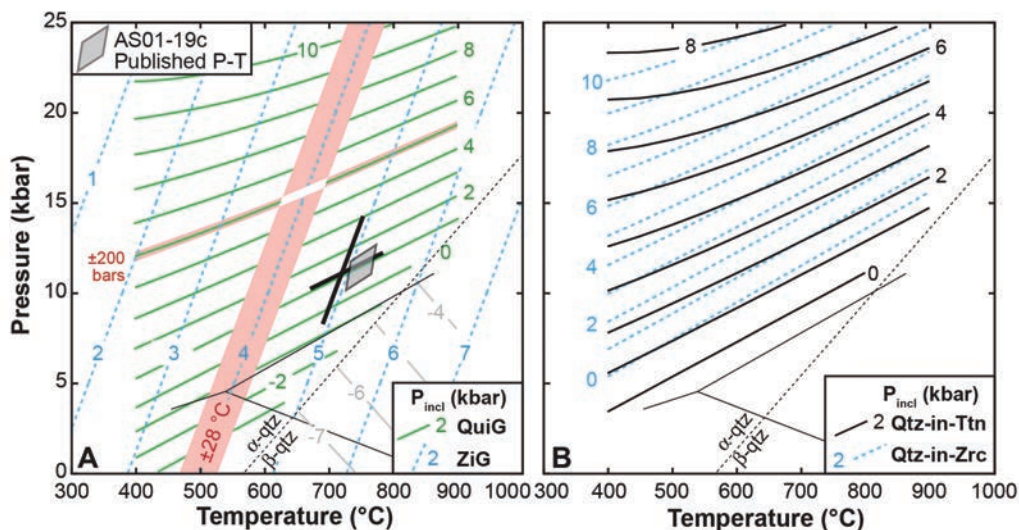


FIGURE 14. (a) Calibration of the quartz-in-garnet (QuiG) and zircon-in-garnet (ZiG) thermobarometers (Kohn 2014a). Example of thermoba-Raman-try for rock from central Himalaya, Nepal (J. Walters and M. Kohn, unpubl. data) shows close correspondence with conventional thermobarometry (Corrie and Kohn 2011). (b) Calibration of the quartz-in-titanite and quartz-in-zircon barometers (Kohn 2014a), illustrating good barometric potential (closely spaced, flat isopleths).

(Parkinson and Katayama 1999; Guiraud and Powell 2006; Kohn 2014a; see also Ye et al. 2001; Korsakov et al. 2010), the quartz-in-zircon, quartz-in-titanite, and quartz-in-rutile barometers appear promising (Fig. 14b). These specific barometers are potentially quite useful. For example, zircon ages from quartz-bearing domains analyzed by Kaneko et al. (2003; Fig. 3) could in principle be coupled with Ti-in-zircon temperatures and quartz-in-zircon pressures to determine specific *P-T-t* points. Such observations would define better both the prograde *P-T* path and rates of subduction and heating. Similarly quartz inclusions in Himalayan titanite could be used to identify rates of burial or exhumation during protracted heating. In contrast, Zr-modeling and regional geochronology suggest that quartz inclusions in zircons from the Scandinavian Caledonides would help constrain retrograde *P-T* conditions and exhumation rates. In this context, the greatest power of thermobarometry may lie in identifying pressures, rather than temperatures, of inclusion entrapment. In many petrologic and tectonic interpretations, metamorphic depths and how they change through time prove more useful than temperature. Possibly thermobarometry will help fill this gap in our petrochronologic toolbox.

ACKNOWLEDGMENTS

Thanks are due Jesse Walters for measuring Raman spectra on quartz and zircon inclusions in the Himalayan garnet, to Frank Spear and an anonymous reviewer for helpful comments, and to Frank Spear for collecting X-ray maps on the Chilean garnet. Funded by NSF grants EAR1048124 and EAR1321897.

REFERENCES CITED

- Ague, J.J., and Baxter, E.F. (2007) Brief thermal pulses during mountain building recorded by Sr diffusion in apatite and multicomponent diffusion in garnet. *Earth and Planetary Science Letters*, 261, 500–516.
- Arevalo, R.J., and McDonough, W.F. (2010) Chemical variations and regional diversity observed in MORB. *Chemical Geology*, 271, 70–85.
- Ashley, K.T., Caddick, M.J., Steele-MacInnis, M.J., Bodnar, R.J., and Dragovic, B. (2014) Geothermobarometric history of subduction recorded by quartz inclusions in garnet. *Geochemistry, Geophysics, Geosystems*, 15, 350–360.
- Beckman, V., Möller, C., Söderlund, U., Corfu, F., Pallon, J., and Chamberlain, K.R. (2014) Metamorphic zircon formation at the transition from gabbro to eclogite in Trollheimen-Surnadalen, Norwegian Caledonides. *Geological Society, London, Special Publications*, 390, 403–424.
- Berman, R.G. (1988) Internally-consistent thermodynamic data for minerals in the system Na₂O-K₂O-CaO-MgO-FeO-Fe₂O₃-Al₂O₃-SiO₂-TiO₂-H₂O-CO₂. *Journal of Petrology*, 29, 445–522.
- Berman, R.G., and Aranovich, L.Y. (1996) Optimized standard state and solution properties of minerals 1. Model calibration for olivine, orthopyroxene, cordierite, garnet, and ilmenite in the system FeO-MgO-CaO-Al₂O₃-TiO₂-SiO₂. *Contributions to Mineralogy and Petrology*, 126, 1–24.
- Boehnke, P., Watson, E.B., Trail, D., Harrison, T.M., and Schmitt, A.K. (2013) Zircon saturation re-visited. *Chemical Geology*, 351, 324–334.
- Burton, K.W., Kohn, M.J., Cohen, A.S., and O'Nions, R.K. (1995) The relative diffusion of Pb, Nd, Sr and O in garnet. *Earth and Planetary Science Letters*, 133, 199–211.
- Carlson, W.D. (2006) Rates of Fe, Mg, Mn, and Ca diffusion in garnet. *American Mineralogist*, 91, 1–11.
- Carosi, R., Montomali, C., Rubatto, D., and Visona, D. (2013) Leucogranite intruding the South Tibetan Detachment in western Nepal: implications for exhumation models in the Himalayas. *Terra Nova*, 25, 478–489.
- Carswell, D.A., Tucker, R.D., O'Brien, P.J., and Krogh, T.E. (2003) Coesite micro-inclusions and the U/Pb age of zircons from the Hareidland eclogite in the Western Gneiss Region of Norway. *Lithos*, 67, 181–190.
- Catlos, E.J., Harrison, T.M., Kohn, M.J., Grove, M., Ryerson, F.J., Manning, C.E., and Upreti, B.N. (2001) Geochronological and thermobarometric constraints on the evolution of the Main Central Thrust, central Nepal Himalaya. *Journal of Geophysical Research-Solid Earth*, 106, 16177–16204.
- Cherniak, D.J. (1993) Lead diffusion in titanite and preliminary results on the effects of radiation damage on Pb transport. *Chemical Geology*, 110, 177–194.
- (2000) Pb diffusion in rutile. *Contributions to Mineralogy and Petrology*, 139, 198–207.
- (2006) Zr diffusion in titanite. *Contributions to Mineralogy and Petrology*, 152, 639–647.
- Cherniak, D.J., and Watson, E.B. (1992) A study of strontium diffusion in K-feldspar, Na-K feldspar and anorthite using Rutherford backscattering spectroscopy. *Earth and Planetary Science Letters*, 113, 411–425.
- (1994) A study of strontium diffusion in plagioclase using Rutherford backscattering spectroscopy. *Geochimica et Cosmochimica Acta*, 58, 5179–5190.
- (2001) Pb diffusion in zircon. *Chemical Geology*, 172, 5–24.
- (2007) Ti diffusion in zircon. *Chemical Geology*, 242, 470–483.
- Cherniak, D.J., Watson, E.B., Grove, M., and Harrison, T.M. (2004) Pb diffusion in monazite: a combined RBS/SIMS study. *Geochimica et Cosmochimica Acta*, 68, 207–226.
- Cherniak, D.J., Manchester, J., and Watson, E.B. (2007) Zr and Hf diffusion in rutile. *Earth and Planetary Science Letters*, 261, 267–279.
- Chernoff, C.B., and Carlson, W.D. (1999) Trace element zoning as a record of chemical disequilibrium during garnet growth. *Geology*, 27, 555–558.
- Chorlton, L.B., and Martin, R.F. (1978) The effect of boron on the granite solidus. *Canadian Mineralogist*, 16, 239–244.
- Corrie, S.L., and Kohn, M.J. (2008) Trace-element distributions in silicates during prograde metamorphic reactions: implications for monazite formation. *Journal of Metamorphic Geology*, 26, 451–464.
- (2011) Metamorphic history of the central Himalaya, Annapurna region, Nepal, and implications for tectonic models. *Geological Society of America Bulletin*, 123, 1863–1879.
- Corrie, S.L., Kohn, M.J., and Vervoort, J.D. (2010) Young eclogite from the Greater Himalayan Sequence, Arun Valley, eastern Nepal: P-T path and tectonic implications. *Earth and Planetary Science Letters*, 289, 406–416.
- Cottle, J.M., Searle, M.P., Horstwood, M.S.A., and Waters, D.J. (2009a) Timing of midcrustal metamorphism, melting, and deformation in the Mount Everest region of southern Tibet revealed by U(-Th)-Pb geochronology. *Journal of Geology*, 117, 643–664.
- Cottle, J.M., Jessup, M.J., Newell, D.L., Horstwood, M.S.A., Noble, S.R., Parrish, R.R., Waters, D.J., and Searle, M.P. (2009b) Geochronology of granulitized eclogite from the Ama Drime Massif: Implications for the tectonic evolution of the South Tibetan Himalaya. *Tectonics*, 28, TC1002.
- Dempster, T.J., Hay, D.C., Gordon, S.H., and Kelly, N.M. (2008) Micro-zircon: origin and evolution during metamorphism. *Journal of Metamorphic Geology*, 26, 499–507.
- Dodson, M.H. (1986) Closure profiles in cooling systems. *Materials Science Forum*, 7, 145–154.
- Enami, M., Nishtyama, T., and Mouri, T. (2007) Laser Raman microspectrometry of metamorphic quartz: A simple method for comparison of metamorphic pressures. *American Mineralogist*, 92, 1303–1315.
- Engl, M. (2009) Petrochronology in the Central Alps: Results, implications, gaps. *Mineralogical Society of Great Britain and Ireland Annual Meeting Abstracts with Program*.
- Fraser, G., Ellis, D., and Eggins, S. (1997) Zirconium abundance in granulite-facies minerals, with implications for zircon geochronology in high-grade rocks. *Geology*, 25, 607–610.
- Ganguly, J., Tirone, M., and Hervig, R.L. (1998) Diffusion kinetics of samarium and neodymium in garnet, and a method for determining cooling rates of rocks. *Science*, 281, 805–807.
- Ganguly, J., Dasgupta, S., Cheng, W., and Neogi, S. (2000) Exhumation history of a section of the Sikkim Himalayas, India: records in the metamorphic mineral equilibria and compositional zoning of garnet. *Earth and Planetary Science Letters*, 183, 471–486.
- Gardés, E., Montel, J.-M., Seydoux-Guillaume, A.-M., and Wirth, R. (2007) Pb diffusion in monazite: New constraints from the experimental study of Pb²⁺ ↔ Ca²⁺ interdiffusion. *Geochimica et Cosmochimica Acta*, 71, 4036–4043.
- Gebauer, D., Schertl, H.P., Brix, M., and Schreyer, W. (1997) 35 Ma old ultrahigh-pressure metamorphism and evidence for very rapid exhumation in the Dora Maira Massif, Western Alps. *Lithos*, 41, 5–24.
- Godin, L., Grujic, D., Law, R.D., and Searle, M.P. (2006) Channel flow, ductile extrusion and exhumation in continental collision zones: an introduction. *Geological Society Special Publication*, 268, 1–23.
- Gordon, S.M., Whitney, D.L., Teysseier, C., and Fossen, H. (2013) U-Pb dates and trace-element geochemistry of zircon from migmatite, Western Gneiss Region, Norway: Significance for history of partial melting in continental subduction. *Lithos*, 170–171, 35–53.
- Gromet, L.P., Dymek, R.F., Haskin, L.A., and Korotev, R.L. (1984) The “North American shale composite”; its compilation, major and trace element characteristics. *Geochimica et Cosmochimica Acta*, 48, 2469–2482.
- Grove, M., and Harrison, T.M. (1999) Monazite Th-Pb age depth profiling. *Geology*, 27, 487–490.
- Guiraud, M., and Powell, R. (2006) P-V-T relationships and mineral equilibria in inclusions in minerals. *Earth and Planetary Science Letters*, 244, 683–694.
- Guo, Z., and Wilson, M. (2012) The Himalayan leucogranites: Constraints on the nature of their crustal source region and geodynamic setting. *Gondwana Research*, 22, 360–376.
- Hames, W.E., and Menard, T. (1993) Fluid-assisted modification of garnet composition along rims, cracks, and mineral inclusion boundaries in samples of amphibolite facies schists. *American Mineralogist*, 78, 338–344.

- Harris, N., and Massey, J. (1994) Decompression and anatexis of Himalayan metapelites. *Tectonics*, 13, 1537–1546.
- Harris, N.B.W., Caddick, M., Kosler, J., Goswami, S., Vance, D., and Tindle, A.G. (2004) The pressure-temperature-time path of migmatites from the Sikkim Himalaya. *Journal of Metamorphic Geology*, 22, 249–264.
- Hayden, L.A., Watson, E.B., and Wark, D.A. (2008) A thermobarometer for sphene (titanite). *Contributions to Mineralogy and Petrology*, 155, 529–540.
- Herman, F., Copeland, P., Avouac, J.-P., Bollinger, L., Mahéo, G., Le Fort, P., Rai, S., Foster, D., Pecher, A., Stüwe, K., and Henry, P. (2010) Exhumation, crustal deformation, and thermal structure of the Nepal Himalaya derived from inversion of thermochemical and thermobarometric data and modeling of the topography. *Journal of Geophysical Research*, 115, <http://dx.doi.org/10.1029/2008/JB006126>.
- Hoisch, T.D., Wells, M.L., and Grove, M. (2008) Age trends in garnet-hosted monazite inclusions from upper amphibolite-facies schist in the northern Grouse Creek Mountains, Utah. *Geochimica et Cosmochimica Acta*, 72, 5505–5520.
- Holland, T.J.B., and Powell, R. (1998) An internally consistent thermodynamic data set for phases of petrological interest. *Journal of Metamorphic Geology*, 16, 309–343.
- Imayama, T., Takeshita, T., Keewook, Y., Cho, D.-L., Kitajima, K., Tsutsumi, Y., Kayama, M., Nishido, H., Okumura, T., Yagi, K., Itaya, T., and Sano, Y. (2012) Two-stage partial melting and contrasting cooling history within the Higher Himalayan Crystalline Sequence in the far-eastern Nepal Himalaya. *Lithos*, 134–135, 1–22.
- Inger, S., and Harris, N.B.W. (1992) Tectonothermal evolution of the High Himalayan crystalline sequence, Langtang Valley, northern Nepal. *Journal of Metamorphic Geology*, 10, 439–452.
- Izraeli, E.S., Harris, J.W., and Navon, O. (1999) Raman barometry of diamond formation. *Earth and Planetary Science Letters*, 173, 351–360.
- Janots, E., Brunet, F., Goffé, B., Poinssot, C., Burchard, M., and Cemič, L. (2007) Thermochemistry of monazite-(La) and dissakisite-(La): implications for monazite and allanite stability in metapelites. *Contributions to Mineralogy and Petrology*, 154, 1–14.
- Kaneko, Y., Katayama, I., Yamamoto, H., Misawa, K., Ishikawa, M., Rehman, H.U., Kausar, A.B., and Shiraiishi, K. (2003) Timing of Himalayan ultrahigh-pressure metamorphism: sinking rate and subduction angle of the Indian continental crust beneath Asia. *Journal of Metamorphic Geology*, 21, 589–599.
- Kellett, D.A., Grujic, D., Coutand, I., Cottle, J., and Mukul, M. (2013) The South Tibetan detachment system facilitates ultra rapid cooling of granulite-facies rocks in Sikkim Himalaya. *Tectonics*, 32, <http://dx.doi.org/10.1002/tect.20014>.
- Kelly, N.M., Clarke, G.L., and Harley, S.L. (2006) Monazite behaviour and age significance in poly-metamorphic high-grade terrains: A case study from the western Musgrave Block, central Australia. *Lithos*, 88, 100–134.
- Kelsey, D.E., and Powell, R. (2011) Progress in linking accessory mineral growth and breakdown to major mineral evolution in metamorphic rocks: a thermodynamic approach in the Na₂O-CaO-K₂O-FeO-MgO-Al₂O₃-SiO₂-H₂O-TiO₂-ZrO₂ system. *Journal of Metamorphic Geology*, 29, 151–166.
- Kelsey, D.E., Clark, C., and Hand, M. (2008) Thermobarometric modelling of zircon and monazite growth in melt-bearing systems: examples using model metapelitic and metapsammitic granulites. *Journal of Metamorphic Geology*, 26, 199–212.
- Ketcham, R.A. (2005) Forward and inverse modeling of low-temperature thermochronometry data. *Reviews in Mineralogy and Geochemistry*, 58, 275–314.
- Kohn, M.J. (2004) Oscillatory- and sector-zoned garnets record cyclic (?) rapid thrusting in central Nepal. *Geochemistry, Geophysics, Geosystems*, 5, 10.1029/2004gc000737.
- (2008) P-T-t data from central Nepal support critical taper and repudiate large-scale channel flow of the Greater Himalayan Sequence. *Geological Society of America Bulletin*, 120, 259–273.
- (2013) Geochemical zoning in metamorphic minerals. In R. Rudnick, Ed., *Treatise on Geochemistry, The Crust*, 3, p. 229–261. Elsevier, Amsterdam.
- (2014a) “Thermobar-Raman-try”: Calibration of spectroscopic barometers and thermometers for mineral inclusions. *Earth and Planetary Science Letters*, 388, 187–196.
- (2014b) Himalayan metamorphism and its tectonic implications. *Annual Review of Earth and Planetary Sciences*, 42, 381–419.
- Kohn, M.J., and Corrie, S.L. (2011) Preserved Zr-temperatures and U-Pb ages in high-grade metamorphic titanite: evidence for a static hot channel in the Himalayan orogen. *Earth and Planetary Science Letters*, 311, 136–143.
- Kohn, M.J., and Malloy, M.A. (2004) Formation of monazite via prograde metamorphic reactions among common silicates: Implications for age determinations. *Geochimica et Cosmochimica Acta*, 68, 101–113.
- Kohn, M.J., and Spear, F.S. (1991a) Error propagation for barometers: 1. Accuracy and precision of experimentally located end-member reactions. *American Mineralogist*, 76, 128–137.
- (1991b) Error propagation for barometers: 2. Application to rocks. *American Mineralogist*, 76, 138–147.
- Kohn, M.J., Catlos, E.J., Ryerson, F.J., and Harrison, T.M. (2001) Pressure-temperature-time path discontinuity in the Main Central thrust zone, central Nepal. *Geology*, 29, 571–574.
- Kohn, M.J., Wieland, M.S., Parkinson, C.D., and Upreti, B.N. (2004) Miocene faulting at plate tectonic velocity in the Himalaya of central Nepal. *Earth and Planetary Science Letters*, 228, 299–310.
- Kohn, M.J., Wieland, M.S., Parkinson, C.D., and Upreti, B.N. (2005) Five generations of monazite in Langtang gneisses: implications for chronology of the Himalayan metamorphic core. *Journal of Metamorphic Geology*, 23, 399–406.
- Kohn, M.J., Corrie, S.L., and Markley, C. (2015) The fall and rise of metamorphic zircon. *American Mineralogist*, 100, 897–908.
- Korsakov, A.V., Zhukov, V.P., and Vandenebee, P. (2010) Raman-based geobarometry of ultrahigh-pressure metamorphic rocks: applications, problems, and perspectives. *Analytical and Bioanalytical Chemistry*, 397, 2739–2752.
- Kouketsu, Y., Nishiyama, T., Ikeda, T., and Enami, M. (2014) Evaluation of residual pressure in an inclusion-host system using negative frequency shift of quartz Raman spectra. *American Mineralogist*, 99, 433–442.
- Krogh, T.E., Kamo, S.L., Robinson, P., Terry, M.P., and Kwok, K. (2011) U-Pb zircon geochronology of eclogites from the Scandian Orogen, northern Western Gneiss Region, Norway: 14–20 million years between eclogite crystallization and return to amphibolite-facies conditions. *Canadian Journal of Earth Science*, 48, 441–472.
- Kylander-Clark, A.R.C., Hacker, B.R., Johnson, C.M., Beard, B.L., and Mahlen, N.J. (2009) Slow subduction of a thick ultrahigh-pressure terrane. *Tectonics*, 28, <http://dx.doi.org/10.1029/2007TC002251>.
- Langille, J.M., Jessup, M.J., Cottle, J.M., Lederer, G., and Ahmad, T. (2012) Timing of metamorphism, melting and exhumation of the Leo Pargil dome, northwest India. *Journal of Metamorphic Geology*, 30, 769–791.
- Lapen, T.J., Johnson, C.M., Baumgartner, L.P., Mahlen, N.J., Beard, B.L., and Amato, J.M. (2003) Burial rates during prograde metamorphism of an ultrahigh-pressure terrane: an example from Lago di Cignana, western Alps, Italy. *Earth and Planetary Science Letters*, 215, 57–72.
- Lasaga, A.C. (1983) Geospeedometry: An extension of geothermometry. In S.K. Saxena, Ed., *Kinetics and Equilibrium in Mineral Reactions*, p. 81–114. Springer-Verlag, New York.
- Li, D.W., Liao, Q.N., Yuan, Y.M., Wan, Y.S., Liu, D.M., Zhang, X.H., Yi, S.H., Cao, S.Z., and Xie, D.F. (2003) SHRIMP U-Pb zircon geochronology of granulites at Rimana (Southern Tibet) in the central segment of Himalayan Orogen. *Chinese Science Bulletin*, 48, 2647–2650.
- Liu, Z.-C., Wu, F.Y., Ji, W.Q., Wang, J.-G., and Liu, C.-Z. (2014) Petrogenesis of the Ramba leucogranite in the Tethyan Himalaya and constraints on the channel flow model. *Lithos*, 208–209, 118–136.
- Martin, A.J., Gehrels, G.E., and DeCelles, P.G. (2007) The tectonic significance of (U,Th)/Pb ages of monazite inclusions in garnet from the Himalaya of central Nepal. *Chemical Geology*, 244, 1–24.
- Martin, L.A.J., Balleve, M., Boulvais, P., Halfpenny, A., Vanderhaeghe, O., Duchene, S., and Delouale, E. (2011) Garnet re-equilibration by coupled dissolution–reprecipitation: evidence from textural, major element and oxygen isotope zoning of ‘cloudy’ garnet. *Journal of Metamorphic Geology*, 29, 213–231.
- Montel, J.-M. (1993) A model for monazite/melt equilibrium and application to the generation of granitic magmas. *Chemical Geology*, 110, 127–146.
- Najman, Y., Appel, E., Boudagher-Fadel, M., Bown, P., Carter, A., Garzanti, E., Godin, L., Han, J., Liebke, U., Oliver, G., Parrish, R., and Vezzoli, G. (2010) Timing of India-Asia collision: Geological, biostratigraphic, and palaeomagnetic constraints. *Journal of Geophysical Research*, 115, <http://dx.doi.org/10.1029/2010JB007673>.
- Neogi, S., Dasgupta, S., and Fukuoka, M. (1998) High P-T polymetamorphism, dehydration melting, and generation of migmatites and granulites in the Higher Himalayan Crystalline Complex, Sikkim, India. *Journal of Petrology*, 39, 61–99.
- Parkinson, C.D., and Katayama, I. (1999) Present-day ultrahigh-pressure conditions of coesite inclusion in zircon and garnet: Evidence from laser Raman microspectroscopy. *Geology*, 27, 979–982.
- Pattison, D.R.M., De Capitani, C., and Gaidies, F. (2011) Petrological consequences of variations in metamorphic reaction affinity. *Journal of Metamorphic Geology*, 29, 953–977.
- Pollok, K., Lloyd, G.E., Austrheim, H., and Putnis, A. (2008) Complex replacement patterns in garnets from Bergen Arcs eclogites: a combined EBSD and analytical TEM study. *Chemie der Erde*, 68, 177–191.
- Putnis, A. (2002) Mineral replacement reactions: from macroscopic observations to microscopic mechanisms. *Mineralogical Magazine*, 66, 689–708.
- Pyle, J.M., and Spear, F.S. (1999) Yttrium zoning in garnet: coupling of major and accessory phases during metamorphic reactions. *Geological Materials Research*, 1, 1–49.
- (2003) Four generations of accessory-phase growth in low-pressure migmatites from SW New Hampshire. *American Mineralogist*, 88, 338–351.
- Pyle, J.M., Spear, F.S., Rudnick, R.L., and McDonough, W.F. (2001) Monazite-xenotime-garnet equilibrium in metapelites and a new monazite-garnet thermometer. *Journal of Petrology*, 42, 2083–2107.
- Rapp, R.P., Ryerson, F.J., and Miller, C.F. (1987) Experimental evidence bearing on the stability of monazite during crustal anatexis. *Geophysical Research Letters*, 14, 307–310.
- Root, D.B., Hacker, B.R., Mattinson, J.M., and Wooden, J.L. (2004) Zircon geochronology and ca. 400 Ma exhumation of Norwegian ultrahigh-pressure

- rocks: an ion microprobe and chemical abrasion study. *Earth and Planetary Science Letters*, 228, 325–341.
- Rosenfeld, J.L., and Chase, A.B. (1961) Pressure and temperature of crystallization from elastic effects around solid inclusions in minerals? *American Journal of Science*, 259, 519–541.
- Rubatto, D. (2002) Zircon trace element geochemistry: partitioning with garnet and link between U-Pb ages and metamorphism. *Chemical Geology*, 184, 123–138.
- Rubatto, D., Chakraborty, S., and Dasgupta, S. (2013) Timescales of crustal melting in the Higher Himalayan Crystallines (Sikkim, Eastern Himalaya) inferred from trace element-constrained monazite and zircon chronology. *Contributions to Mineralogy and Petrology*, 165, 349–372.
- Sano, Y., Terada, K., and Fukuoka, T. (2002) High mass resolution ion microprobe analysis of rare earth elements in silicate glass, apatite, and zircon: lack of matrix dependency. *Chemical Geology*, 184, 217–230.
- Scaillet, B., France-Lanord, C., and Le Fort, P. (1990) Badrinath-Gangotri plutons (Garhwal, India): petrological and geochemical evidence for fractionation processes in a high Himalayan leucogranite. *Journal of Volcanology and Geothermal Research*, 44, 163–188.
- Searle, M.P., and Fryer, B.J. (1986) Garnet, tourmaline and muscovite-bearing leucogranites, gneisses and migmatites of the Higher Himalayas from Zaskar, Kulu, Lahoul and Kashmir. In M.P. Coward and A.C. Ries, Eds., *Collision Tectonics*, 19, p. 185–201. Geological Society Special Publication, London.
- Smith, H.A., and Giletti, B.J. (1997) Lead diffusion in monazite. *Geochimica et Cosmochimica Acta*, 61, 1047–1055.
- Smye, A.J., and Stockli, D.F. (2014) Rutile U-Pb age depth profiling: a continuous record of lithospheric thermal evolution. *Earth and Planetary Science Letters*, 408, 171–182.
- Smye, A.J., Stöckli, D.F., and Zack, T. (2014) Tracing lithospheric thermal evolution with high field strength element speedometry in rutile. *EOS—Transactions of the American Geophysical Union*, V54B-08.
- Sobolev, N.V., Fursenko, B.A., Goryainov, S.V., Shu, J.F., Hemley, R.J., Mao, H.K., and Boyd, F.R. (2000) Fossilized high pressure from the Earth's deep interior: The coesite-in-diamond barometer. *Proceedings of the National Academy of Sciences*, 97, 11875–11879.
- Spear, F.S. (2004) Fast cooling and exhumation of the Valhalla metamorphic core complex, southeastern British Columbia. *International Geology Review*, 46, 193–209.
- (2010) Monazite-allanite phase relations in metapelites. *Chemical Geology*, 279, 55–62.
- Spear, F.S., and Kohn, M.J. (1996) Trace element zoning in garnet as a monitor of crustal melting. *Geology*, 24, 1099–1102.
- Spear, F.S., and Pyle, J.M. (2010) Theoretical modeling of monazite growth in a low-Ca metapelite. *Chemical Geology*, 273, 111–119.
- Spear, F.S., Kohn, M.J., and Cheney, J.T. (1999) P-T paths from anatectic pelites. *Contributions to Mineralogy and Petrology*, 134, 17–32.
- Spear, F.S., Thomas, J.B., and Hallett, B.W. (2014) Overstepping the garnet isograd: a comparison of QuiG barometry and thermodynamic modeling. *Contributions to Mineralogy and Petrology*, 168, 1059.
- Spencer, K.J., Hacker, B.R., Kylander-Clark, A.R.C., Andersen, T.B., Cottle, J.M., Stearns, M.A., Poletti, J.E., and Seward, G.G.E. (2013) Campaign-style titanite U-Pb dating by laser-ablation ICP: Implications for crustal flow, phase transformations and titanite closure. *Chemical Geology*, 341, 84–101.
- Stübner, K., Grujic, D., Parrish, R.R., Roberts, N.M.W., Kronz, A., Wooden, J., and Ahmad, T. (2014) Monazite geochronology unravels the timing of crustal thickening in the NW Himalaya. *Lithos*, 210–211, 111–128.
- Terry, M.P., Robinson, P., Hamilton, M.A., and Jercinovic, M.J. (2000) Monazite geochronology of UHP and HP metamorphism, deformation, and exhumation, Nordøyane, Western Gneiss Region, Norway. *American Mineralogist*, 85, 1651–1664.
- Thompson, R. (1969) Àbátán: A master potter of the Ègbádò Yorùbá. In D. Biebuyck, Ed., *Tradition and Creativity in Tribal Art*, p. 120–182. University of California Press, Berkeley.
- Thöni, M., Miller, C., Hager, C., Grasemann, B., and Horschinegg, M. (2012) New geochronological constraints on the thermal and exhumation history of the Lesser and Higher Himalayan Crystalline Units in the Kullu-Kinnaur area of Himachal Pradesh (India). *Journal of Asian Earth Sciences*, 52, 98–116.
- Tomkins, H.S., Powell, R., and Ellis, D.J. (2007) The pressure dependence of the zirconium-in-rutile thermometer. *Journal of Metamorphic Geology*, 25, 703–713.
- Vielzeuf, D., Veschambre, M., and Brunet, F. (2005) Oxygen isotope heterogeneities and diffusion profile in composite metamorphic-magmatic garnets from the Pyrenees. *American Mineralogist*, 90, 463–472.
- Vry, J.K., and Baker, J.A. (2006) LA-MC-ICPMS Pb-Pb dating of rutile from slowly cooled granulites: Confirmation of the high closure temperature for Pb diffusion in rutile. *Geochimica et Cosmochimica Acta*, 70, 1807–1820.
- Walther, J.V., and Wood, B.J. (1984) Rate and mechanism in prograde metamorphism. *Contributions to Mineralogy and Petrology*, 88, 246–259.
- Wang, J.M., Zhang, J.J., and Wang, X.X. (2013) Structural kinematics, metamorphic P-T profiles and zircon geochronology across the Greater Himalayan Crystalline Complex in south-central Tibet: implication for a revised channel flow. *Journal of Metamorphic Geology*, 31, 607–628.
- Watson, E.B., and Harrison, T.M. (1983) Zircon saturation revisited; temperature and composition effects in a variety of crustal magma types. *Earth and Planetary Science Letters*, 64, 295–304.
- Watson, E.B., Wark, D.A., and Thomas, J.B. (2006) Crystallization thermometers for zircon and rutile. *Contributions to Mineralogy and Petrology*, 151, 413–433.
- Whitehouse, M.J., and Platt, J.P. (2003) Dating high-grade metamorphism—constraints from rare-earth elements in zircon and garnet. *Contributions to Mineralogy and Petrology*, 145, 61–74.
- Yakymchuk, C., and Brown, M. (2014) Behaviour of zircon and monazite during crustal melting. *Journal of the Geological Society, London*, 171, 465–479.
- Yang, P., and Rivers, T. (2001) Chromium and manganese zoning in pelitic garnet and kyanite; spiral, overprint, and oscillatory (?) zoning patterns and the role of growth rate. *Journal of Metamorphic Geology*, 19, 455–474.
- (2002) The origin of Mn and Y annuli in garnet and the thermal dependence of P in garnet and Y in apatite in calc-pelite and pelite, Gagnon terrane, western Labrador. *Geological Materials Research*, 4, <http://gmr.minsocam.org/contents.html>.
- Ye, K., Liou, J.B., Cong, B.L., and Maruyama, S. (2001) Overpressures induced by coesite-quartz transition in zircon. *American Mineralogist*, 86, 1151–1155.
- Young, D.J., Hacker, B.R., Andersen, T.B., and Corfu, F. (2007) Prograde amphibolite facies to ultrahigh-pressure transition along Nordfjord, western Norway: Implications for exhumation tectonics. *Tectonics*, 26, <http://dx.doi.org/10.1029/2004TC001781>.
- Young, D.J., Hacker, B.R., Andersen, T.B., and Gans, P.B. (2011) Structure and ⁴⁰Ar/³⁹Ar thermochronology of an ultrahigh-pressure transition in western Norway. *Journal of the Geological Society*, 168, 887–898.
- Zeng, L., Gao, L.-E., Dong, C., and Tang, S. (2012) High-pressure melting of metapelite and formation of Ca-rich granitic melts in the Namche Barwa Massif, southern Tibet. *Gondwana Research*, 21, 138–151.
- Zhang, Y.X. (1998) Mechanical and phase equilibria in inclusion-host systems. *Earth and Planetary Science Letters*, 157, 209–222.

MANUSCRIPT RECEIVED JULY 31, 2014

MANUSCRIPT ACCEPTED FEBRUARY 23, 2015

MANUSCRIPT HANDLED BY EDWARD GHENT